The developmental and genetic basis of 'clubfoot' in the peroneal muscular atrophy mutant mouse

Collinson, J. M., Lindström, N. O., Neves, C., Wallace, K., Meharg, C., Charles, R. H., Ross, Z. K., Fraser, A. M., Mbogo, I., Oras, K., Nakamoto, M., BArker, S., Duce, S., Miedzybrodzka, Z., & Vargesson, N. (2018). The developmental and genetic basis of 'clubfoot' in the peroneal muscular atrophy mutant mouse. *Development (Cambridge, England)*, *145*(3), [dev160093]. https://doi.org/10.1242/dev.160093

Published in:
Development (Cambridge, England)

Document Version:
Publisher's PDF, also known as Version of record

© 2018. Published by The Company of Biologists Ltd | Development (2018) 145, dev160093. doi:10.1242/dev.160093

RESEARCH ARTICLE

The developmental and genetic basis of 'clubfoot' in the peroneal muscular atrophy mutant mouse

J. Martin Collinson[1,‡‡], Nils O. Lindström[1,*], Carlos Neves[1], Karen Wallace[1], Caroline Meharg[1,‡], Rebecca H. Charles[1], Zoe K. Ross[1], Amy M. Fraser[1,§], Ivan Mbogo[1,¶], Kadri Oras[1,], Masaru Nakamoto[1], Simon Barker[2], Suzanne Duce[3], Zosia Miedzybrodzka[1] and Neil Vargesson[1]**

ABSTRACT

Genetic factors underlying the human limb abnormality congenital talipes equinovarus ('clubfoot') remain incompletely understood. The spontaneous autosomal recessive mouse 'peroneal muscular atrophy' mutant (PMA) is a faithful morphological model of human clubfoot. In PMA mice, the dorsal (peroneal) branches of the sciatic nerves are absent. In this study, the primary developmental defect was identified as a reduced growth of sciatic nerve lateral motor column (LMC) neurons leading to failure to project to dorsal (peroneal) lower limb muscle blocks. The *pma* mutation was mapped and a candidate gene encoding LIM-domain kinase 1 (*Limk1*) identified, which is upregulated in mutant lateral LMC motor neurons. Genetic and molecular analyses showed that the mutation acts in the EphA4–Limk1–Cfl1/cofilin–actin pathway to modulate growth cone extension/collapse. In the chicken, both experimental upregulation of *Limk1* by electroporation and pharmacological inhibition of actin turnover led to defects in hindlimb spinal motor neuron growth and pathfinding, and mimicked the clubfoot phenotype. The data support a neuromuscular aetiology for clubfoot and provide a mechanistic framework to understand clubfoot in humans.

KEY WORDS: Limk1, Axon guidance, Clubfoot, Limb development, Chicken

INTRODUCTION

Congenital talipes equinovarus (CTEV, also known as 'clubfoot') is a human lower limb developmental defect with a worldwide prevalence of 1-3 cases for every 1000 live births, making it one of the most common pediatric orthopedic conditions (Cartlidge, 1984; Dobbs et al., 2000). Clubfoot is characterised by the inward rotation and downward flexion of the foot, which persists after birth and, unless corrected, causes permanent disability. However, our understanding of the aetiological and genetic factors underlying clubfoot is incomplete. Most clubfoot births, where the infant has unilateral or bilateral CTEV but no other clinical problems, are largely unexplained. Most patients respond well to serial casting (Ponseti manipulation) followed by Achilles tenotomy in infancy but a significant proportion (10-15%) experience relapse and most post-clubfoot individuals experience some degree of leg fatigue (Ippolito et al., 2009).

Several hypotheses have been put forward to explain clubfoot aetiology. Although intuitively clubfoot may be assumed to arise from a skeletal patterning defect, there is in fact little evidence for this and the primary defect appears to be hindlimb developmental arrest from around day 44 of gestation (Miedzybrodzka, 2003). The hindlimb must rotate during late embryogenesis, such that the sole of the foot, which lies initially in the plane of the body axis, faces down, with toes lying in the horizontal plane. Clubfoot results when this rotation fails to complete, and it has been hypothesised that a musculoskeletal inter-relationship is required for limb rotation (Isaacs et al., 1977; Stewart, 1951; Bechtol and Mossman, 1950; Dittrich, 1930; Ponseti and Campos, 1972). Several lines of clinical evidence show that weakness, inactivity, or absence of calf muscles can be associated with clubfoot (Flynn et al., 2007; Ohno et al., 1986), and there is persistent loss of muscle density in the calves of individuals with clubfoot (Duce et al., 2013).

Twin studies and population genetics have provided strong evidence for a genetic basis of clubfoot (Miedzybrodzka, 2003). Complex segregation analyses suggest that the most likely inheritance pattern is a single gene of major effect but low penetrance, with either dominant or recessive inheritance, operating against a polygenic background (Wang et al., 1988; de Andrade et al., 1988; Rebbeck et al., 1993; Chapman et al., 2000). However, the identity of the major gene(s) involved remains elusive. Mutations in the genes encoding the hindlimb transcription factors *PITX1* and *TBX4* have been shown to lead to a reduction in lower limb musculature and classic clubfoot phenotypes in humans and mice, although these may also be associated with syndromic long bone growth defects (Gurnett et al., 2008; Alvarado et al., 2010, 2011; Lu et al., 2012; Peterson et al., 2014). Approximately 5% of human cases of familial isolated clubfoot are associated with microduplications of *TBX4* (Dobbs and Gurnett, 2013). There are other mouse models [e.g. ephrin receptor *EphA4* knockout mice exhibit clubfoot as part of a syndrome of motor and cognitive abnormalities (Helmbacher et al., 2000)] but none of these has led to the discovery of other major human causative genes, and most cases of clubfoot in humans are idiopathic (i.e. with no known cause).

A spontaneous mouse mutant, the peroneal muscular atrophy (PMA) mouse, shows an inherited, hindlimb-restricted, bilateral clubfoot-like phenotype at birth that is comparable to the human

[1]School of Medicine, Medical Sciences and Nutrition, University of Aberdeen, Institute of Medical Sciences, Foresterhill, Aberdeen AB25 2ZD, UK. [2]Royal Aberdeen Children's Hospital, Foresterhill, Aberdeen AB25 2ZN, UK. [3]School of Life Sciences, University of Dundee, Dundee DD1 5EH, UK.
*Present address: Eli and Edythe Broad CIRM Center for Regenerative Medicine and Stem Cell Research at USC, 1425 San Pablo Street, BCC 312, Los Angeles, CA 90033-9080, USA. ‡Present address: Institute For Global Food Security, Queen's University Belfast, Belfast, Northern Ireland. §Present address: Division of Developmental Biology, Roslin Institute, University of Edinburgh, Easter Bush, Edinburgh, UK. ¶Present address: Evolutionary Neurobiology Unit, Okinawa Institute of Science and Technology Graduate University, 1919-1 Tancha, Onnason, Okinawa, 904-0495, Japan. **Present address: Department of Genetics, University of Cambridge, Downing Street, Cambridge CB2 3EH, UK.

‡‡Author for correspondence (m.collinson@abdn.ac.uk)

J.M.C., 0000-0002-8111-475X

Received 23 October 2017; Accepted 28 December 2017

Development (2018) 145, dev160093. doi:10.1242/dev.160093

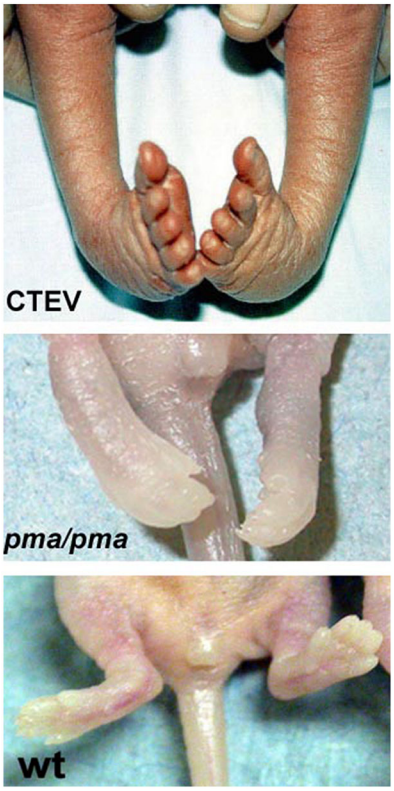

Fig. 1. Clubfoot phenotype in *pma*/*pma* mice. Human newborn with congenital talipes equinovarus (CTEV, commonly known as clubfoot) (top) compared with newborn *pma*/*pma* mouse (middle) and newborn wild-type mouse (bottom).

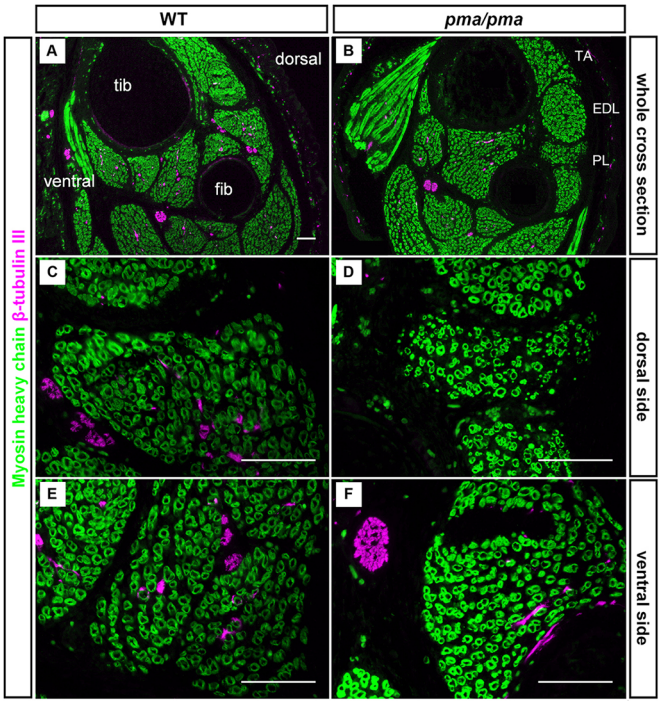

Fig. 2. Absence of innervation of dorsal (peroneal) calf muscles in *pma*/*pma* homozygotes. Immunohistochemistry of cross-sections of stage-matched E16.5 wild-type (WT; left) and *pma*/*pma* homozygotes (right) using antibodies against myosin heavy chain to label muscle blocks (green) and β-III-tubulin to label nerves (red). (A,B) Low-magnification images with ventral muscles to the left and dorsal muscles to the right. (C,D) Higher-magnification images of dorsal muscle blocks showing innervation of wild-type dorsal muscles (C) but not of dorsal muscles in *pma*/*pma* homozygotes (D). (E,F) Magnification of ventral muscles showing innervation of both wild-type (E) and *pma*/*pma* (F) mice EDL, extensor digitorum longus; fib, fibula; PL, peroneus longus; TA, tibialis anterior; tib, tibia. Scale bars: 25 µm.

pathology (Nonaka et al., 1986; Duce et al., 2010) (Fig. 1). The mutation is autosomal recessive with high penetrance, and has been previously mapped to mouse chromosome 5 (Katoh et al., 2003). However, no candidate gene has been identified and at least 67 genes are contained within the 4.8 Mb mapped region. Adult *pma/pma* mice have anterior-lateral regional defects of the hindlimbs only, including absence of the peroneal nerve and atrophy of the anterior-lateral calf muscle compartment (Nonaka et al., 1986; Ashby et al., 1993). It is hypothesised that, because the outer (dorsal and lateral) calf muscles are atrophied but the inner (ventral and posterior) are normal, the foot remains in a CTEV-like position during development. It is not known why the peroneal branch of the sciatic nerve fails in PMA mice. Normally, the motor neurons that contribute to the sciatic nerve project from the lateral motor columns (LMCs) of the ventral neural tube. Those that will contribute to dorsal limb nerves project from the lateral LMC (lLMC), whereas those that will project ventrally originate in the medial region of the LMC (mLMC) (Landmesser, 1978). Both populations project through the ventral roots of the lumbar neural tube and coalesce at the lumbosacral plexus before entering the hindlimb (Wang and Scott, 2008; Jessell, 2000). Here, they branch into the ventral limb, becoming the precursors of the tibial and sural nerves, or into the dorsal limb, becoming the peroneal nerve.

The PMA mouse is potentially a clinically relevant model of clubfoot, but the genetic basis of the phenotype has not been described, and the primary defect, whether developmental or degenerative, is poorly understood. This work explores the aetiology and genetics of clubfoot using the PMA animal model. By genetic mapping, sequencing and gene expression analysis, we identify *Limk1* as a candidate gene underlying the *pma* mutation and show, using mouse and chicken models, that overexpression of this gene delays neuronal growth and drives aberrant neuron guidance, resulting in muscular defects, failure of foot rotation, and clubfoot.

RESULTS

Peroneal nerve development is aborted in *pma*/*pma* embryos

It has been shown previously that the common peroneal nerve is absent in adult *pma/pma* mice (Nonaka et al., 1986). This is the dorsal branch of the sciatic nerve that innervates the anterior-dorsal 'peroneal' calf muscles, which are atrophied in the PMA mouse and in patients with clubfoot (Duce et al., 2010, 2013). Immunohistochemistry on tissue sections and whole-mount preparations at embryonic day (E)16.5 confirmed the complete absence of motor innervation in the dorsal-anterior muscles of the lower leg of *pma/pma* homozygotes (the tibialis anterior, the extensor digitorum longus and the peroneus longus), with normal innervation of ventral calf muscles (Fig. 2). Immunohistochemical analysis showed that the anterior-dorsal muscles were normally vascularised in *pma/pma* homozygotes (Fig. S1). The data confirm that the clubfoot phenotype in PMA mice is associated with neural rather than vascular failure. To define the earliest developmental stage at which a defect is observed, homozygous *pma/pma* mouse embryos were examined histologically at E10.5-E16.5. It was found that, at E11.5, the sciatic nerve had entered the hindlimb of wild-

Development (2018) 145, dev160093. doi:10.1242/dev.160093

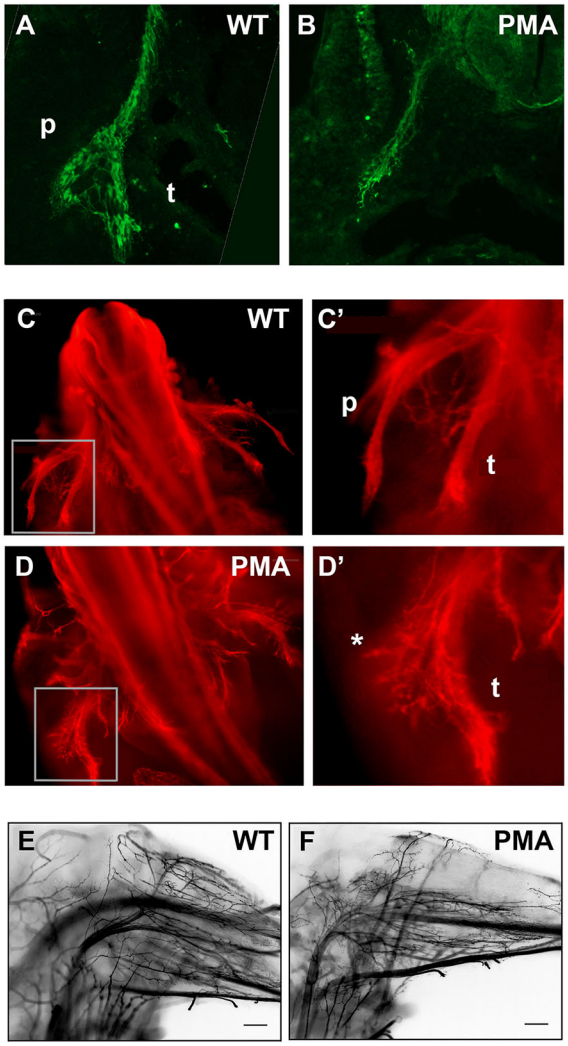

Fig. 3. Retardation of nerve growth and abortive innervation of dorsal muscles in PMA mice. (A,B) β-III-tubulin immunohistochemistry (green) in transverse sections of stage-matched E11.75 wild-type (WT; A) and *pma*/*pma* mice (B). The wild-type sciatic nerve has projected further than that in the *pma*/*pma* mice and, unlike the PMA nerve, started to branch into discrete dorsal (peroneal, p) and ventral (tibial/sural, t) components. (C,D) Whole-mount β-III-tubulin immunohistochemistry (red) on wild-type (C,C′) and *pma*/*pma* (D,D′) embryos. C′ and D′ show magnifications of the boxed areas over the left-hand-side nerves in C and D, respectively. The peroneal (p) and tibial/sural (t) components are labelled. In *pma*/*pma* embryos, the tibial/sural branch is grossly normal, but only a few defasciculated axons are observable (asterisk) in place of the peroneal nerve, presenting a feather-like appearance. (E,F) Whole-mount β-III-tubulin immunohistochemistry on lower hindlimbs of E16.5 wild-type (left) and *pma*/*pma* embryos (right). Dorsal is to top: the dorsal muscles of the *pma*/*pma* foetuses are completely aneural, suggesting that the putative peroneal axons noted at E12.5 have not survived. Scale bars: 50 µm.

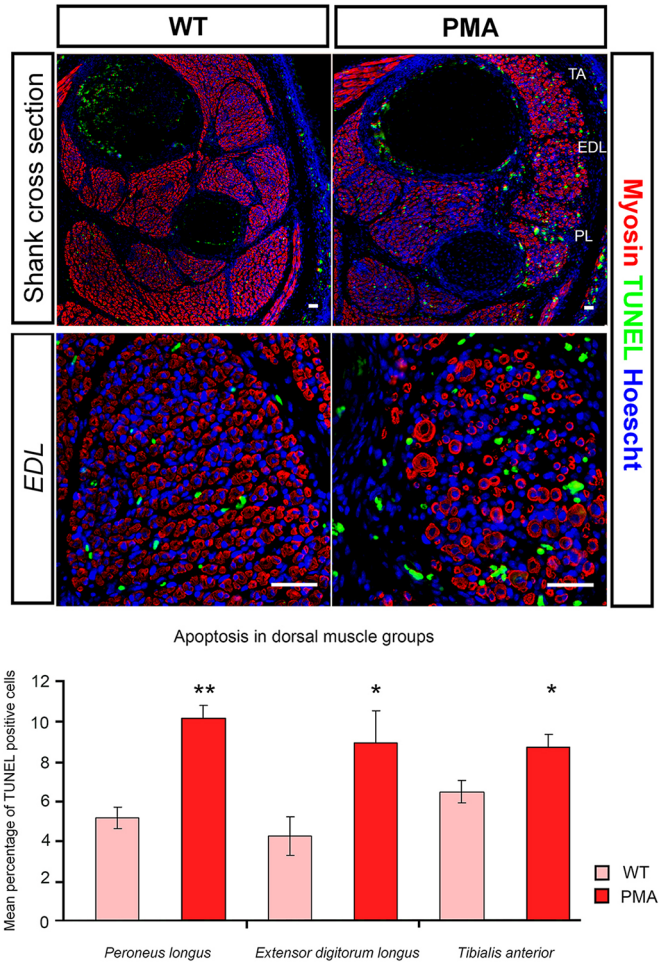

Fig. 4. Increased apoptosis in dorsal muscle blocks of the pma hindlimb. Top: TUNEL labelling (green) to visualise apoptotic cells in cross-sections of E16.5 wild-type (WT; left) and *pma*/*pma* foetuses (right), combined with immunohistochemistry for myosin heavy chain (red) and Hoechst nuclear stain (blue). Higher magnification of the one dorsal muscle, the extensor digitorum longus, is shown. Bottom: Although apoptosis occurs in all muscles, the percentage of TUNEL-positive cells was significantly greater in the three major dorsal muscle blocks of *pma*/*pma* foetuses than in wild-type controls (n=8 for both groups). *P<0.05; **P<0.01. Error bars represent s.e.m. Scale bars: 50 µm.

type mouse homozygotes and the beginnings of branching were visible, but in stage-matched *pma/pma* homozygote embryos, the nerve had neither entered the limb nor started to branch (Fig. 3A,B). At E12.5, wild-type sciatic nerves had forked into clearly demarcated, fasciculated dorsal peroneal and ventral tibial trunks (Fig. 3C,C′). The E12.5 *pma/pma* littermates had a morphologically normal tibial trunk and no obvious peroneal nerve, suggesting failure of normal branching. However, whole-mount immunohistochemistry showed a dorsal projection of a small number of defasciculated axons projecting dorsally in E12.5 *pma/pma* embryos that may represent an abortive peroneal nerve (Fig. 3D,D′). The fate of these axons is unknown, because no peroneal innervation was detectable at later stages, as described above (Fig. 3E,F). The peroneal nerve was confirmed by dissection to be absent postnatally in *pma/pma* mice, consistent with the observations of Nonaka et al. (1986) (Fig. S2).

We previously observed degeneration of the peroneal muscles in adult *pma/pma* hindlimbs (Duce et al., 2010). To determine whether this was secondary to the loss of innervating nerves, we scrutinised early muscle development in *pma/pma* limbs. Abnormal myotube structures were observed specifically in myosin-positive developing dorsal muscles only at E16.5, with an approximate twofold increase in apoptosis (Fig. 4). These results confirmed at a molecular level the previous observations of regional muscular defects in PMA mice by our and other groups (Nonaka et al., 1986; Ashby et al., 1993; Duce et al., 2010) and showed that muscle failure occurred subsequent to failure of innervation.

Development (2018) 145, dev160093. doi:10.1242/dev.160093

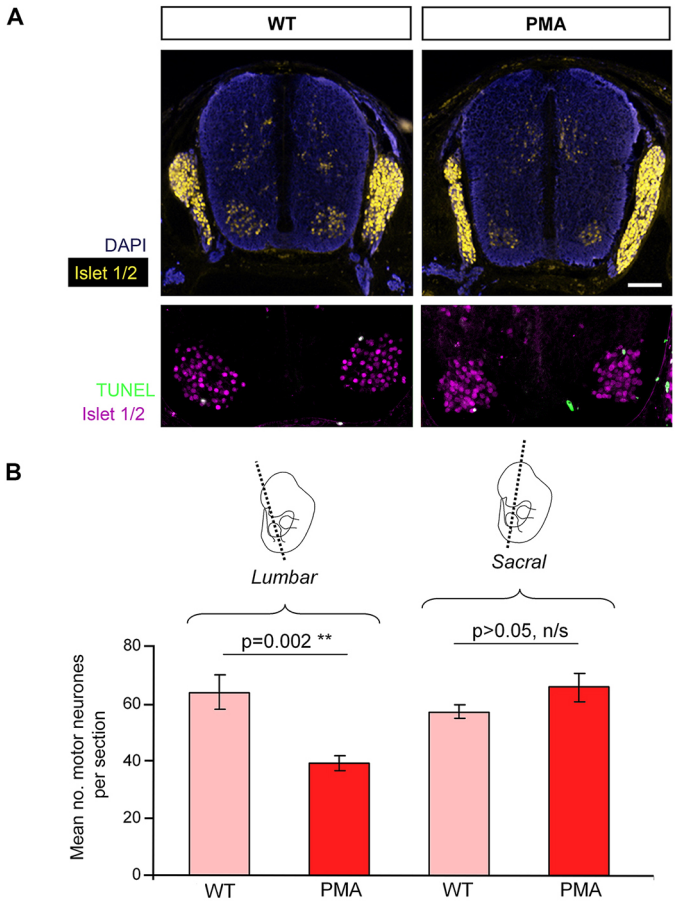

Fig. 5. Apoptosis and motor neuron survival in lumbar neural tube of *pma/pma* homozygotes. (A) Immunohistochemistry on cross-sections of lumbar neural tube of E14.5 wild-type (WT; left) and *pma/pma* (right) foetuses. Islet 1 staining (yellow/magenta) is evident in the dorsal root ganglia and more weakly so in the lateral motor columns of both genotypes. There are rare apoptotic events in both genotypes (TUNEL labelling, green) but quantification was not possible as so few apoptotic cells were detected. (B) Quantification of motor neuron numbers in the neural tube of E16.5 wild-type and *pma/pma* foetuses. There are significantly fewer surviving motor neurons in *pma/pma* foetuses specifically at the level of the hindlimb (lumbar) but not more posteriorly (sacral). Error bars represent s.e.m. n/s, not significant. Scale bar: 50 µm.

Molecular specification is normal but axon growth is reduced and apoptosis increased in PMA motor neurons

To delineate whether the eventual absence of the peroneal nerve in PMA mice resulted from either the death of putative dorsal-projecting LMC neurons or their misdirection, we measured the cross-sectional area of the sciatic nerve in adult *pma/pma* and wild-type mice of equal weight. The mean area of the *pma/pma* nerve ($98.98\pm0.43\times10^3$ µm^2; n=5) was significantly reduced compared with controls ($111.41\pm1.37\times10^3$ µm^2; n=9; t-test, P=0.014), suggesting that motor neuron death occurred. Although terminal deoxynucleotidyl transferase dUTP nick end labelling (TUNEL) labelling at E11.5-E14.5 revealed no gross abnormal apoptotic events (Fig. 5A), by E16.5 the number of lumbar LMC nuclei was reduced in *pma/pma* homozygotes compared with wild-type stage-matched controls (Fig. 5B). Sacral LMC neurons were not affected. Patterns of proliferation were investigated by bromodeoxyuridine (BrdU) labelling and immunohistochemistry and were found to be normal in *pma/pma* embryos at E11.5 (Fig. S3), suggesting dorsal motor neuron death at E14.5-E16.5, secondary to failure to target the dorsal muscle blocks.

Sciatic motor neurons of the hindlimb are derived from the LMC of the developing lumbar neural tube. The dorsal (peroneal) branch of the sciatic nerve is derived from neurons of the lateral component of the LMC (lLMC), which are characterised by expression of genes encoding marker LIM homeodomain proteins Lim1 (also known as Lhx1) and Islet 2 (Isl2), and the ventral (tibial/sural) branch is derived from the medial LMC neurons (mLMC) expressing Islet 1 and 2 (reviewed by Jessell, 2000). Lim1-deficient lLMCs project illicitly along the ventral pathway (Kania et al., 2000). Dorsoventral patterning of the neural tube and specification of the lLMC and mLMC were investigated in *pma/pma* mice. No defects of patterning were found: the dorsal and mediolateral markers Pax3 and Pax6, respectively, were localised normally from E11.5 to E14.5 (Fig. 6A). The molecular identity of the LMC populations was found to be maintained in *pma/pma* embryos: Lim1-positive lLMC neurons that should form the peroneal nerve were present as normal (Fig. 6B). These data suggest that any loss of peroneal neurons in the *pma/pma* sciatic nerve is not a primary failure of patterning or cell proliferation at E11.5-E12.5, but is secondary to the cellular changes that prevent normal patterns of axonal projection.

No defects in genes required for normal dorsoventral patterning of the hindlimb mesenchyme were detected in E11.5-E12.5 *pma/pma* embryos by western blot or qPCR (Fig. S4). To investigate whether the motor neurons of the PMA mouse were inherently defective, E11.5 lLMCs were dissected from stage-matched *pma/pma* and wild-type embryos and cultured in identical media for 72 h. Immunocytochemical analysis showed projecting axons with β-III-tubulin and cell body localisation of Lim1, confirming their lLMC identity (Fig. 6C,D). Time-lapse measurement of growth cone position showed that *pma/pma* axons projected at approximately half the speed (2.09 µm/100 min; n=50) of wild-type axons (4.03 µm/100 min; n=97) (Fig. 6E, Fig. S5). These data confirm an autonomous defect of *pma/pma* motor neurons.

The data suggest an autonomous qualitative axon growth defect of motor neurons in *pma/pma* embryos, such that limb innervation is delayed. The reasons why this leads to failure of the peroneal branch but not of the tibial/sural are discussed below, but it is postulated that dorsal-specified axons miss their permissive time window for successful projection into the limb. It was concluded that the *pma* mutation has arisen in a gene required for normal extension and ultimate survival of lumbar motor neuron axons.

Genetic mapping of the *pma* mutation

The *pma* mutation was previously mapped to a 4.8 Mb region of chromosome 5 (Katoh et al., 2003). This region contains 67 genes with no standout clubfoot candidate. Genomic PCR was performed for 20 genes spanning the candidate region in *pma/pma* animals and all genes were found to be present, suggesting no large deletion (Fig. S6). We repeated the mapping using a higher density of microsatellites across the candidate region (full details described in supplementary Materials and Methods). The results are presented in Table 1. There were 12 potentially informative crossovers identified, which located the mutation to 2.5 Mb bounded by D5Mit166 (Chr5:133146598-133146706 bp) and D5Mit60 (Chr5:135715435-135715564 bp) (Fig. 7). This smaller candidate region contained 39 genes.

To further define the candidate region, targeted next-generation resequencing was performed on two recombinant mice (one with crossover distal to the mutation, and one with crossover proximal to the mutation), three parental *pma/pma* and three parental BALB/c mice. A 3.04 Mb stretch encompassing the entire candidate region between D5Mit166 and D5Mit60 was obtained from all mice. The

Development (2018) 145, dev160093. doi:10.1242/dev.160093

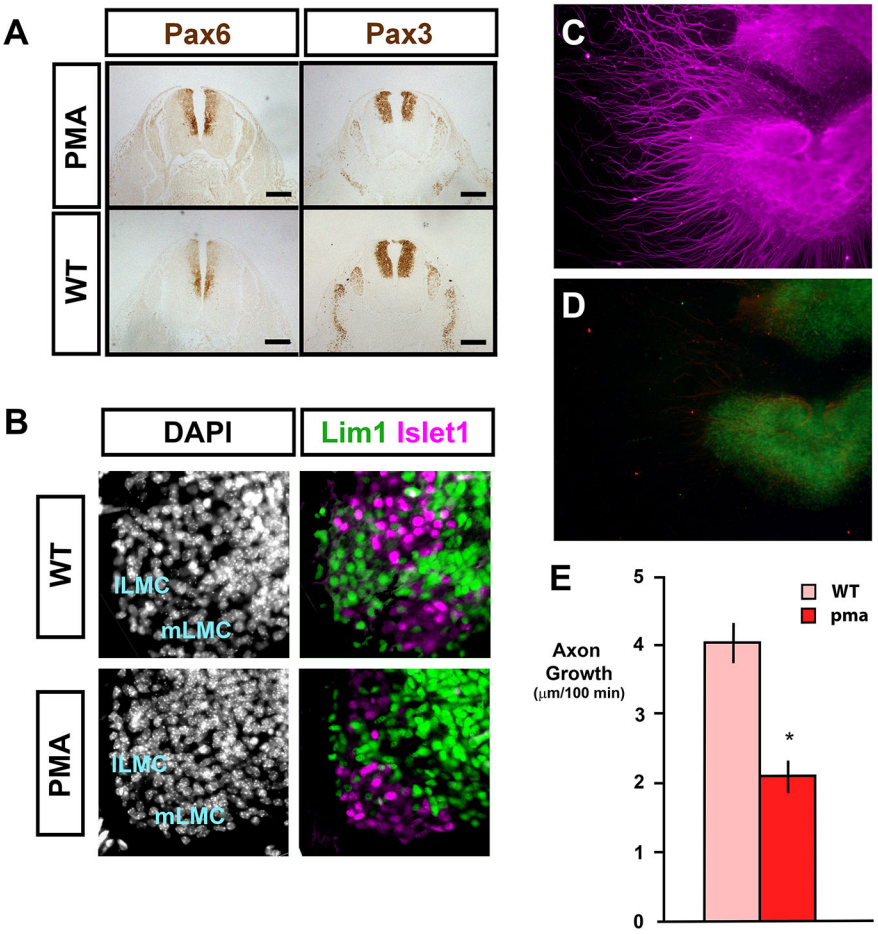

Fig. 6. Normal neural tube patterning but reduced extension of motor neurons in the *pma*/*pma* hindlimb. (A) Immunohistochemistry on cross-sections of the neural tube at E11.5 in *pma*/*pma* embryos and stage-matched wild-type (WT) controls. *Pax6* most strongly labels medial-ventral progenitors at the level of the motor neurons. *Pax3* is localised to more-dorsal progenitors. Both genes are expressed normally in PMA mice and there is no evidence of dorsalisation of the neural tube or loss of motor neuron identity. (B) Immunohistochemistry for the lLMC marker Lim1 (green) and the mLMC marker Islet1 (magenta) at E12.5 in wild-type and *pma*/*pma* stage-matched embryos. Lim1-positive neurons are observable in the *pma*/*pma* lLMC, indicating that peroneal-fated neurons are correctly specified. DAPI nuclear counterstain is shown separately. There is some encroachment of Islet1-positive cells into the lLMC, but green Lim1-positive cells are discernible within the region of encroachment. (C-E) LMC axon growth in wild-type and *pma*/*pma* cultures. Double immunohistochemistry for β-III-tubulin (C; magenta) and Lim1 (D; green) in a LMC culture from a wild-type embryo. Time-lapse analysis of axon extension in motor neuron cultures (E) showed significantly reduced growth in *pma*/*pma* cultures. (See also Fig. S5.) **P*<0.05. Error bars represent s.e.m. Scale bars: 50 µm.

full data set with details of alleles, location, sequencing depth and reproducibility, and inferred sites of crossovers is presented in Table S1. This analysis defined crossovers at approximate positions Chr5: 134514245 and Chr5: 134483438, representing a 0.89 Mb candidate region containing 13 genes: *Gatsl2*; *Wbscr16* (*Rcc1l*); *Gtf2ird2*; *Ncf1*; *Gtf2i*; *Gtf2ird1*; *Cyln2* (*Clip2*); *Lat2*; *Gm52* (*Syna*); *Rfc2*; *Eif4h*; *Limk1* and *Eln* (Fig. 7). Within this 0.89 Mb candidate region, nearly 4075 SNPs and small insertions or deletions (indels) were identified that were unambiguously homozygous for the *pma* allele in all clubfoot crossover animals and not found in BALB/c mice, any one of which could be the '*pma* mutation'. Restricting the analysis only to predicted nonsynonymous SNPs and indels within annotated genes identified 23 single nucleotide polymorphisms (SNPs) that were predicted to cause changes in either the amino acid sequence of the gene product (five SNPs – Table 2) or the untranslated region (UTR) of the processed mRNA (18 SNPs, all located in 3′ UTR) (Table S2). Nearly all these changes were known SNPs and could be identified as existing in the homozygous state in at least one of the C57BL/6, A/J, AKR/J, FVB/NJ and/or CAST/EiJ inbred strains without causing a clubfoot phenotype. The only novel nonsynonymous coding mutation was found in the *Gm52* gene (Table 2). This gene encodes an envelope glycoprotein (now known as syncytin-A), which is a placenta-specific product required for normal architecture of the syncytiotrophoblast-containing labyrinth (Dupressoir et al., 2009). *Gm52* knockout mice die *in utero* with placental failure, indicating that this gene is a weak functional candidate for the *pma* phenotype. These data suggest that the *pma* phenotype is not associated with an amino acid-coding mutation.

In addition, a microRNA, mmu-miR590-5p, is localised to this region (accession number MIMAT0004895), nesting within *Eif4h* (Fig. S7). No mutation was present within the mature 22 base pair miR sequence.

The possibility of gene amplification or deletion was directly tested. Genomic DNA was isolated from *pma* homozygotes and wild-type controls, and real-time PCR was performed for five primer pairs involving *Cyln2*, *Gtf2ird1*, *Limk1* (two primer sets) and *Pde6b*, a gene 20 Mb outside the candidate region. No change in copy number in PMA mice was detected with any primer combination (Fig. S8).

The data suggested the *pma* mutation is not a null mutation (causing total loss of protein product or activity) in any of the genes in the candidate region. In addition to the lack of novel, potentially pathogenic coding mutations identified by sequencing, published knockout mice exist for ten of the genes, none of which produces a clubfoot phenotype or any other relevant motor neuron defect (Table 2). Furthermore, the *pma* candidate region is syntenic to the region of human chromosome 7 that is heterozygously deleted in patients with Williams–Beuren syndrome (Francke, 1999), a morphological and neurodevelopmental disorder associated with developmental delay, mental retardation and behavioural abnormalities. Williams–Beuren syndrome is not associated with clubfoot (Morris, 1999). Therefore, it was hypothesised that the problem was one of misexpression of one or more genes resulting from a regulatory mutation (i.e. one of the several thousand SNPs and small indels affecting an important enhancer or promoter sequence). This was investigated further, as detailed below.

Development (2018) 145, dev160093. doi:10.1242/dev.160093

Table 1. Microsatellite mapping of *pma* mutation in recombinant mice

	Phenotype	Genotype	D5Mit218	D5Mit166	D5Mit282	D5Mit219	D5Mit60	D5Mit33	D5Mit32	D5Mit97	*n*
BALB/c founder	Normal	WT	128/128	109/109	105/105	122/122	132/132	111/111	124/124	118/118	2
PMA founder	Clubfoot	*pma*/*pma*	91/91	112/112	109/109	133/133	127/127	86/86	137/137	124/124	2
[BALB/c×PMA] F1	Normal	*pma*/+	128/91	109/112	105/109	122/133	132/127	111/86	124/137	118/124	2
[BALB/c×PMA] F1×PMA	Normal	*pma*/+	128/91	109/112	105/109	122/133	132/127	111/86	124/137	118/124	3
[BALB/c×PMA] F1×PMA	Clubfoot	*pma*/*pma*	128/91	109/112	109/109	133/133	127/127	86/86	137/137	124/124	**3**
[BALB/c×PMA] F1×PMA	Clubfoot	*pma*/*pma*	91/91	112/112	109/109	133/133	132/127	111/86	124/137	118/124	**4**
[BALB/c×PMA] F1×PMA	Clubfoot	*pma*/*pma*	91/91	112/112	109/109	133/133	127/127	111/86	124/137	118/124	2
[BALB/c×PMA] F1×PMA	Clubfoot	*pma*/*pma*	91/91	112/112	109/109	133/133	127/127	86/86	124/137	118/124	2
[BALB/c×PMA] F1×PMA	Clubfoot	*pma*/*pma*	91/91	112/112	109/109	133/133	127/127	86/86	137/137	118/124	1
[BALB/c× PMA] F1× PMA	Clubfoot	*pma*/*pma*	91/91	112/112	109/109	133/133	127/127	86/86	137/137	124/124	187

Results of microsatellite genotyping of BALB/c and *pma*/*pma* founders, their F1 progeny (top three rows) and the backcross F2 (bottom seven rows), for eight informative microsatellites as described in Table S5 and the main text, in chromosomal order. Microsatellite allele sizes are given. Red shading indicates homozygosity for the BALB/c alleles. No shading indicates homozygosity for the PMA founder alleles. Pink shading indicates heterozygosity for the BALB/c×PMA alleles. The number of animals tested that showed each phenotype/genotype combination is shown on the right. Numbers in bold indicate informative crossover events proximal or distal to the *pma* mutation that restricted the candidate region to between D5Mit166 and D5Mit60.

Overexpression of *Limk1* in *pma* homozygotes

Of the 13 genes within the mapped region, *Limk1*, *Cyln2* and *Eif4h* were the best candidates to underlie the motor neuron defects in the PMA mouse on account of known or inferred function in central nervous system (CNS) axon guidance. *Limk1* encodes LIM-domain kinase 1, an enzyme that phosphorylates and inactivates the actin-depolymerising protein cofilin (Yang et al., 1998). Limk1 activity modulates growth cone extension/retraction decisions and acts in a biochemical pathway that is downstream of *EphA4*, which was previously shown to be mutated in a clubfoot mouse model (Helmbacher et al., 2000). *Cyln2* encodes the CAP-GLY domain-containing linker protein 2 (also known as CLIP-115), which acts as a microtubule-associate linking protein in the CNS (Hoogenraad et al., 1998, 2000). *Cyln2* was shown to be strongly expressed in the developing motor neurons of the sciatic nerve (Fig. S9). *Eif4h* encodes a neurally expressed translation initiation factor responsible for modulating normal neuronal number and complexity in the CNS (Capossela et al., 2012).

Expression of *Limk1*, *Eifh4* and *Cyln2* was investigated in the PMA mouse by qPCR on cDNA from limbs and neural tubes of E11.5 *pma/pma* embryos and stage-matched wild types (Fig. 8A). No change in *Cyln2* or *EIf4h* expression was detected, but the data suggested variable but significant four- to sevenfold upregulation of

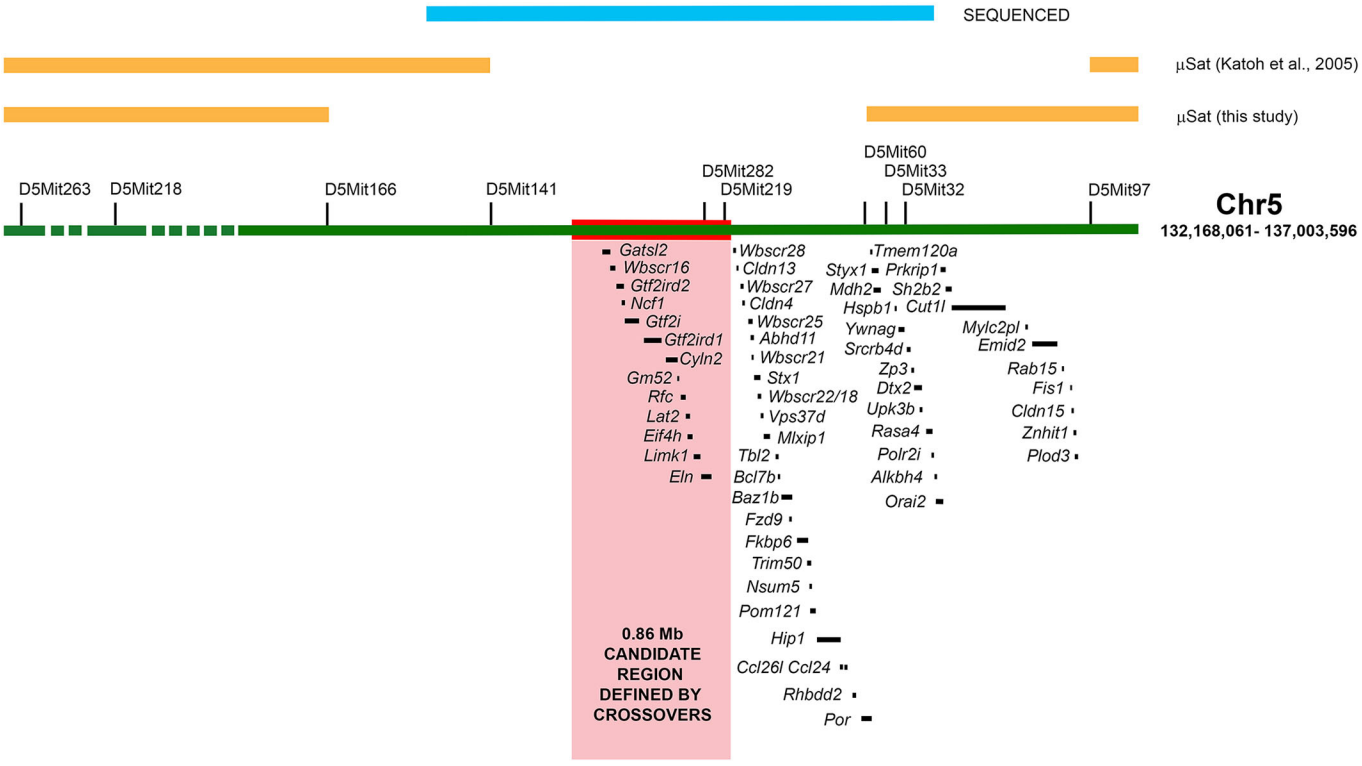

Fig. 7. Genetic mapping of the *pma* mutation. The region of chromosome 5 linked to the *pma* mutation by Katoh et al. (2003) is represented by the green horizontal bar, with the location of all genes listed below. Positions of microsatellites (µSat) used for genetic mapping are shown by black bars. The region eliminated from the candidate area by this study is shown by orange bars (see Table 1), with additional orange bars showing the minimum area defined by Katoh et al. (2003). The 3.04 Mb region sequenced in crossover animals, PMA and BALB/c founders is indicated by the blue bar. The red bar and pink shaded area represent the region within the crossovers identified by sequencing, and delineate a 0.86 Mb region most likely to encompass the *pma* mutation, containing 13 genes.

Development (2018) 145, dev160093. doi:10.1242/dev.160093

Table 2. Thirteen candidate genes identified by mapping and sequencing

Gene	Protein	Function	Amino acid change in PMA	dbSNP	Motor neuron expression	KO phenotype	References
Gatsl2	GATS protein like 2	Cellular arginine sensor for MTORC1 protein				No knockout	Chantranupong et al., 2016
Wbscr16	RCC1-like G-exchanging factor	OPA1-specific guanine nucleotide exchange factor			Y	Embryo lethal	Huang et al., 2017
Gtf2ird2	GTF2I repeat domain-containing transcription factor 2	Cell cycle progression. Muscle fiber type specification	S290N	rs51440048		None known	Porter et al., 2012; Palmer et al., 2012
Ncf1	Neutrophil cytosolic factor 1	Cytosolic subunit of neutrophil NADPH oxidase				Immunocompromised	Jackson et al., 1995
Gtf2i	General transcription factor IIi	Transcription preinitiation complex			Y	Lethality, craniofacial abnormalities, cortical dysmorphology	Enkhmandakh et al., 2009
Gtf2ird1	GTF2I repeat domain-containing transcription factor 1 (BEN)	Positive transcriptional regulator			Y	Craniofacial abnormalities, behavioural change	Bayarsaihan and Ruddle, 2000; Palmer et al., 2010
Cyln2	CAP-Gly domain-containing linker protein 2 (CLIP-115)	Regulation of microtubule dynamics	V25I	rs13486563	Y	Growth deficiency, enlarged ventricular volumes, motor coordination defects	Hoogenraad et al., 2000, 2002
Gm52	Syncytin-A	Fusion of trophoblast cells	H31R	Novel		Placental failure, embryo lethal	Dupressoir et al., 2009
Rfc	Replication factor C subunit 1	DNA replication			Y	Embryo lethal	Dickinson et al., 2016
Lat2	Linker for activation of T cells, transmembrane adaptor 2	Couples innate immune system and B cell receptors to associated kinases				Haematopoietic/immune system failure, mortality	Iwaki et al., 2007
Eif4h	Eukaryotic translation initiation factor 4H	Stimulates RNA helicase activity	N155S	rs13496900	Y	Growth defects, impaired cognitive/behavioural ability	Bandyopadhyay et al., 2013; Capossela et al., 2012
Limk1	LIM-kinase 1	Regulation of actin cytoskeletal dynamics			Y	Heightened locomotor activity, impaired spatial learning, reduced bone mass, altered synaptic morphology	Tursun et al., 2005; Kawano et al., 2013; Meng et al., 2002
Eln	Elastin	Elastic connective tissue component	R704G	rs13496987		Arterial deficiencies, lethal	Wagenseil et al., 2010

'Amino acid change in PMA' indicates the predicted coding change based on identified SNP distinguishing *pma*/*pma* homozygotes from BALB/c (Tables S1, S2). dbSNP, database identification of SNP if previously catalogued; Y, expression in developing motor neurons confirmed in literature.

Limk1 in both the neural tube (P=0.014) and hindlimb (P=0.027) of *pma/pma* homozygotes.

The putative upregulation of *Limk1* was confirmed by immunohistochemistry and western blot on protein extracts of E11.5 neural tube and hindlimbs. Normalised to β-actin, Limk1 and active (phosphorylated) p-Limk1 were localised at higher levels in *pma/pma* neural tubes and hindlimbs compared with stage-matched wild types (Fig. 8B). Furthermore, phosphorylation of the major substrate of Limk1, the actin-depolymerising protein, cofilin, was shown to be higher in *pma/pma* embryos, whereas total cofilin levels were unchanged. Cyln2 levels were also unchanged in *pma/pma* homozygotes. This suggests that the observed increase in Limk1 leads to phosphorylation and inactivation of cofilin, which in turn could impact the dynamics of actin cytoskeleton remodelling in the growth cones of the sciatic nerve.

We next wanted to understand the Limk1 profile throughout progression of clubfoot in the *pma/pma* mice. Repeating the western blots at E11.5-E16.5 showed that the upregulation of Limk1 expression was transient. Limk1 levels were increased in *pma/pma* mice at E11-E12.5, at the time when the peroneal nerve fails to form and enter the hindlimb, but were reduced to wild-type levels by E16.5 (Fig. S10).

To determine whether the upregulation of Limk1 detected by western blot indicated a genuine per-cell overexpression or misexpression of the gene in ectopic locations, immunohistochemistry was performed. In E11.5 wild types, at the level of the lumbar neural tube, Limk1 protein was observed to be present at higher levels in the neural tube, in particular the lLMC, of *pma/pma* homozygotes compared with controls (Fig. 8C). In *pma/pma* embryos processed in parallel with the wild types, there was a general upregulation of the gene, but protein levels were very high in the lLMC in the neurons that form the peroneal branch of the sciatic nerve.

Limk1 protein was found to be differentially localised in the peroneal and tibial branches of the wild-type sciatic nerve at E12.5. Immunohistochemistry showed that, in wild-type embryos, higher levels of p-LIMK1 were present in the dorsal (peroneal) branch of the sciatic nerve compared with the ventral (tibial) branch (Fig. 8D, Fig. S11).

Development (2018) 145, dev160093. doi:10.1242/dev.160093

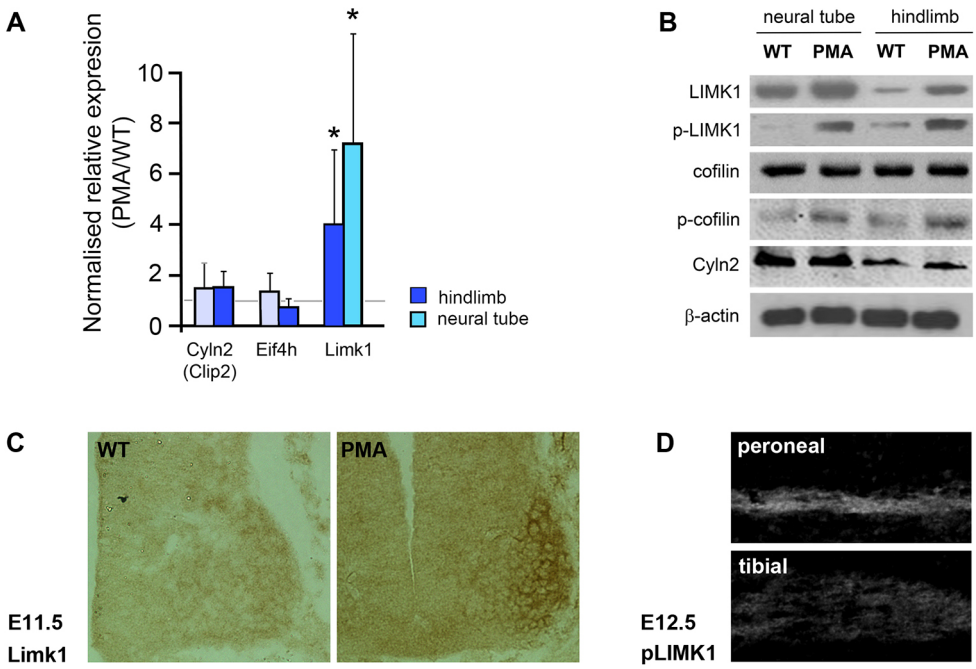

Fig. 8. Upregulation of Lim-kinase 1 (Limk1) in *pma*/*pma* mice. (A) qPCR data of the top-three candidate 'clubfoot' genes in the PMA mouse: *Cyln2*, *Eif4h* and *Limk1*. All data are means from three independent replicates, comparing E11.5 *pma*/*pma* homozygotes with C57BL/6 controls. cDNA was prepared separately from hindlimbs and neural tube of both genotypes. The error bars represent the 95% confidence interval from the statistical randomisation method from the REST software. *Limk1* transcripts were significantly over-represented in both hindlimbs and the neural tube of *pma*/*pma* homozygotes. **P*<0.05. (B) Western blot of E11.5 neural tube and hindlimbs of wild-type (WT) and *pma*/*pma* embryos. Limk1 and p-Limk1 were present at higher levels in *pma*/*pma* homozygotes. Total levels of cofilin (the main substrate of Limk1) were not affected but levels of phosphorylated cofilin increased, as would be expected with upregulation of Limk1. Cyln2 was not affected by *pma* genotype. β-actin was used as the loading control. (C) Immunohistochemistry for Limk1 (brown) in the E11.5 neural tube of wild-type and *pma*/*pma* embryos. Limk1 is present at higher levels in PMA mice, especially in the medial and lateral LMC. (D) Immunohistochemistry for p-Limk1 in dorsal (peroneal) and ventral (tibial) branches of the sciatic nerve at E12.5. p-Limk1 is present at higher levels in the developing peroneal nerve. See also Fig. S11.

Sciatic nerve plexus defects caused by jasplakinolide exposure mimic Limk1 overactivation

Regulatory mutations appear to have an important role in human pathology, particularly in hindlimb deformities (VanderMeer and Ahituv, 2011). Our data suggest that the *pma* mutation is in a *cis*-regulatory element of the *Limk1* gene, increasing its expression.

The predicted consequence of increased Limk1 activity is increased phosphorylation (hence inactivation) of cofilin, leading to inhibition of actin treadmilling in the extending growth cone. This effect can be mimicked pharmacologically using jasplakinolide, a cell-permeable peptide that has been shown to inhibit actin depolymerisation *in vivo* (Bubb et al., 2000; Rosso et al., 2004). For practical purposes, the pharmacological manipulation was performed in chicken embryos: we have recently shown that disruption of neuromuscular function in the hindlimb of chicken embryos causes a clubfoot-like phenotype (N.V., E. Kilby, C.N., S.B., Z.M. and J.M.C., unpublished), establishing the chicken as a useful model of this condition. Jasplakinolide (20 µg/ml) was applied as a microsponge to the dorsal-lumbar region of Hamilton–Hamburger (HH) stage 20-21 chicken embryos *in ovo*, before nerve entry to the limb (approximately equivalent to E10.5 mice). This was followed by whole-mount immunohistochemistry for β-III-tubulin to identify changes in sciatic nerve projection compared with the contralateral untreated limbs and vehicle-treated controls. Axon projection defects were induced after 24 h in 11/29 jasplakinolide-treated limbs but in none of the 15 controls (Fisher exact test: P=0.0079) (Fig. 9). In particular, the rostral-most roots exiting the neural tube, which are the main contributors to the peroneal nerve, were truncated. It was concluded that peroneal nerve disruption is affected by addition of jasplakinolide, consistent with the model that Limk1 overactivation can prevent normal peroneal nerve development *in vivo*.

Electroporation of *Limk1* in chicken neural tube disrupts sciatic nerve innervation of the hindlimb

Electroporation of a plasmid expressing *Limk1* into the lumbar neural tube of stage 11 chicken embryos was performed to experimentally overexpress the gene in hindlimb motor neurons. This caused significant disruption and loss of plexus formation and nerve projection into the limb on the electroporated side of the embryo at stage 24, compared with the contralateral side (Fig. 10A). Electroporation of a control empty vector plasmid had no such effect. Cartilage preparations were made from 12 embryos that were incubated *in ovo* for a further 5 days. Although 9/12 were superficially normal, three showed unilateral clubfoot phenotype on the electroporated side (Fig. 10B). These data confirm that overexpression of Limk1 alone disrupts sciatic nerve formation and suggest that overexpression of Limk1 at the sensitive developmental period leads to clubfoot.

Genetic interaction between *EphA4* mutation and *pma*

EphA4$^{-/-}$ mice show a very high incidence of clubfoot (Helmbacher et al., 2000). Analysis of *EphA4*$^{-/-}$ E16.5 hindlimbs, prior to the failure of limb rotation that characterises clubfoot, showed that only two muscle blocks, the tibialis anterior and the extensor digitorum longus, were aneural, suggesting that the peroneus longus is of lesser consequence for clubfoot (Fig. S12).

Development (2018) 145, dev160093. doi:10.1242/dev.160093

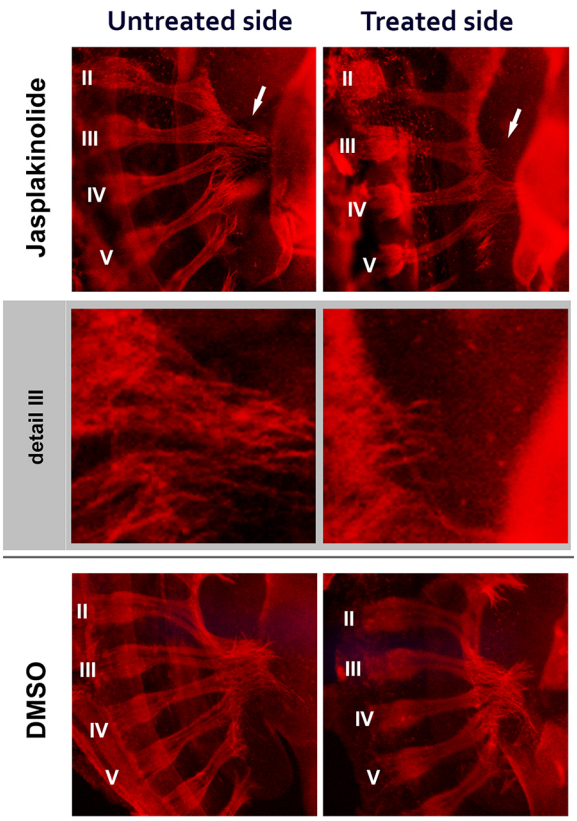

Fig. 9. Jasplakinolide addition to the developing chicken embryo can induce sciatic nerve guidance defects *in vivo*. Whole-mount immunohistochemistry for β-III tubulin 16 h after application of a microsponge containing 20 µg/ml jasplakinolide (or 2% DMSO vehicle) to one side of the HH stage 22-23 chicken embryo at the level of the hindlimb. The spinal cord roots are numbered from I to VI, where root I (not shown) is associated with the anterior femoral nerve and roots III-V contribute to the posterior sciatic nerve. Root VI is only associated with the sciatic nerve later in development. Addition of jasplakinolide induced neuronal defects in the hindlimb. Top row shows jasplakinolide-treated (right) and contralateral untreated (left) sides highlighting the loss of axons on the treated side, especially from rostral-most root III, which contributes to the peroneal nerve (arrows). Shaded in grey is detail from root III. The vehicle, DMSO, was used as a control treatment and no defects were observed (bottom).

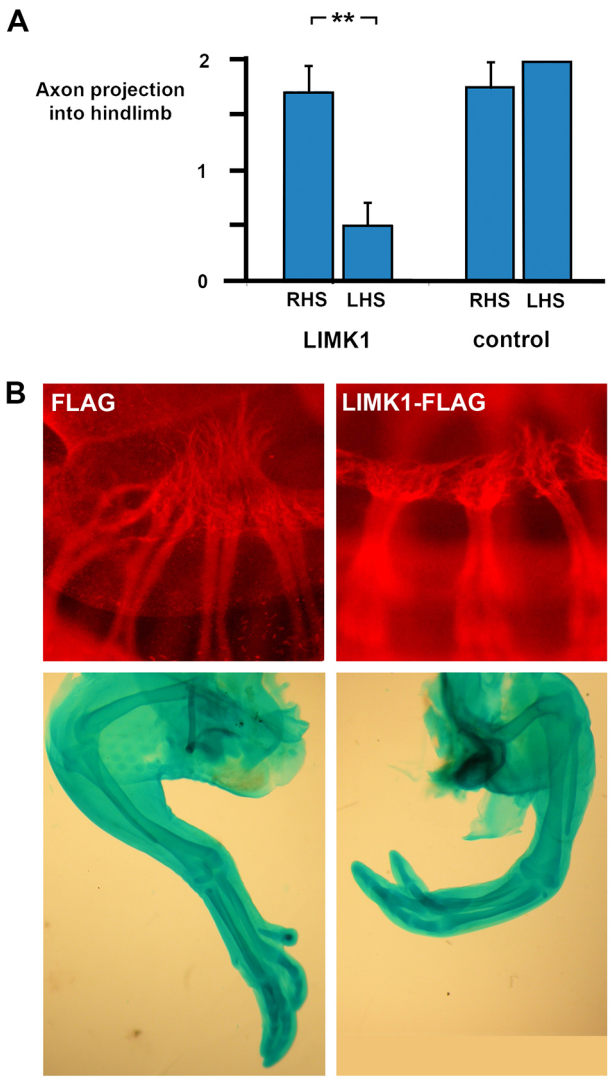

Fig. 10. Electroporation of *LIMK1* into chicken neural tube causes axon loss and clubfoot. Electroporation of plasmids expressing *LIMK1* or empty vector controls into HH stage 11 chickens followed by immunohistochemistry for β-III-tubulin 72 h later or Alcian Blue cartilage staining after a further 5 days. (A) Nerve projection scored 0-2 as described in the Materials and Methods for electroporated (left-hand side, LHS) and non-electroporated contralateral sides (right-hand side, RHS) of each embryo, for *LIMK1* and control vectors, and shows significant inhibition of axon growth in *LIMK1*-treated nerves, but not in empty-vector electroporations. LIMK1 electroporation: RHS nerve score=1.67±0.25, *n*=9; LHS score=0.5±0.22, *n*=8 (one embryo damaged cf. RHS). Control FLAG electroporation: RHS nerve score=1.75±0.25, *n*=4; LHS score=2±0.00, *n*=3. ***P*=0.001 (paired *t*-test). Error bars represent s.e.m. (B) (Top) Whole-mount β-III-tubulin immunohistochemistry (red) on chicken embryos showing normal sciatic plexus formation and axon projection (score 2) after an empty 'FLAG' vector transfection compared with representative failure of nerve plexus formation (score 0) after LIMK1 transfection. (Bottom) Alcian Blue cartilage preparation of (left) a control FLAG-electroporated chicken limb and (right) limb of one of the chickens (3/12) that exhibited a mild clubfoot-like phenotype after transfection with *LIMK1*.

We hypothesised that the *EphA4* mutation acts on the sciatic nerve by modulating the Limk1-cofilin pathway. In support of this, increased labelling of p-cofilin was observed by immunohistochemistry in both E11.5 *pma/pma* and $EphA4^{-/-}$ mice compared with wild-type littermates, consistent with Limk1 regulating cofilin activity (Fig. 11A). To test a genetic interaction between *EphA4* and *pma* mutations, $EphA4^{+/-}$ mice were bred with *pma/pma* homozygotes or wild-type C57BL/6 to generate littermates that were $EphA4^{+/-}$ *pma*/+, $EphA4^{+/+}$ *pma*/+, or $EphA4^{+/+}$ +/+ and $EphA4^{+/-}$ +/+. All progeny were scored as normal, unilateral or bilateral clubfoot at weaning on the basis of gross limb morphology, and dissections were performed to score the presence or absence of the peroneal nerve (Fig. S13). No clubfoot or nerve loss was observed in either $EphA4^{+/+}$ +/+ mice (*n*=37 from these litters) or $EphA4^{+/+}$ *pma*/+ (*n*=44). Mice that were heterozygous only for *EphA4* were usually normal (19/24 mice) but 20.8% (5/24) had unilateral loss of peroneal nerve (either complete loss in four cases or retention of an extremely thin remnant in one case). By contrast, only 32% (12/37) of double heterozygote $EphA4^{+/-}$ *pma*/+ littermates were normal; 45% (17/37) were scored as unilateral clubfoot and showed loss of peroneal nerve on the affected side, whereas 21% (8/37) were bilateral clubfoot with loss or atrophy of nerves (Fig. 11B) (full data set: Table S3). The occurrence of bilateral clubfoot in the double heterozygotes had never been observed in any of the *pma*/+ or $EphA4^{+/-}$ single heterozygotes bred over the course of the project. The increased incidence of peroneal nerve loss in the double heterozygotes was significant (5/24

Development (2018) 145, dev160093. doi:10.1242/dev.160093

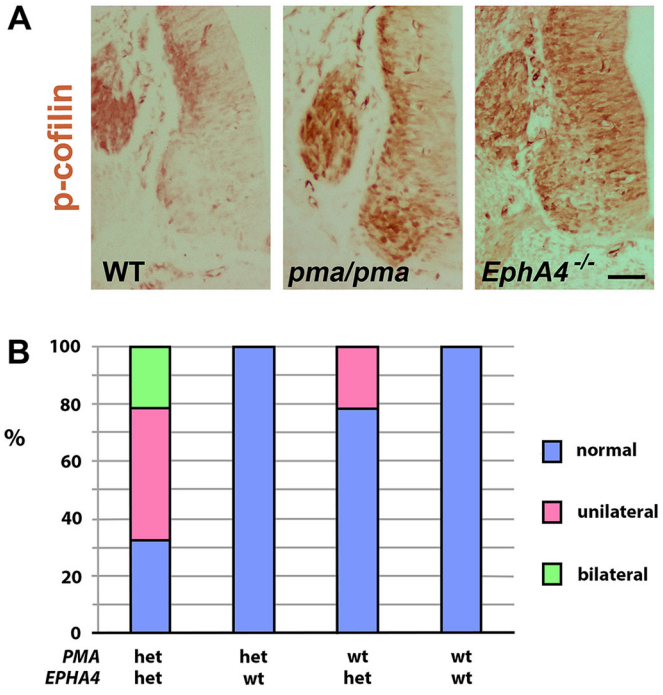

Fig. 11. Interaction between *pma* and *Epha4* mutations. (A) P-cofilin immunohistochemistry (brown) on transverse sections of neural tube of E11.5 wild-type (WT), *pma*/*pma* and *Epha4*$^{-/-}$ mouse embryos. Compared with wild type, p-cofilin is at higher levels in both *pma*/*pma* and *Epha4* mutant mice, suggesting a shared biochemical pathway. Similar levels of protein in the dorsal root ganglia provide an internal control for staining. (B) Representation of frequency occurrence of peroneal nerve loss in postnatal day 21 mice that are compound heterozygotes for *EphA4* and *pma*, compared with single heterozygous littermates for either gene, or littermates wild-type at both loci. See main text for details. Scale bar: 35 µm.

EphA4$^{+/-}$ +/+ mice versus 25/37 *EphA4*$^{+/-}$ *pma*/+. χ^2=12.43, *P*=0.0004). Hence, the phenotype of the double mutation is more severe than the sum of the phenotypes of the single mutations. This is formal genetic evidence that the *pma* mutation lies in the same molecular pathway as *EphA4*. It suggests that the phenotypic occurrence of clubfoot can be associated with the cumulative effect of heterozygosity for predisposing mutations in more than one gene.

DISCUSSION

Clubfoot is a complex heritable abnormality with a range of described anatomical defects and no simple association with any one genetic or environmental factor (Miedzybrodzka, 2003). In this work, the spontaneous autosomal recessive mouse model, peroneal muscular atrophy (PMA), was used to understand the underlying developmental causes of clubfoot. The *pma* mutation was mapped, identifying several candidate genes, of which, *Limk1*, was upregulated in mutant mice. We showed in chickens that *LIMK1* upregulation can cause sciatic nerve defects and a clubfoot phenotype. We also demonstrated proof of principle in mice that expression of the clubfoot phenotype can occur because of the cumulative effect of predisposing alleles at more than one locus.

Limk1 as the *pma* clubfoot gene

We have previously shown that *Limk1* is dynamically expressed during embryogenesis (Lindström et al., 2011). Neural tube expression patterns of *Limk1* and patterns of p-cofilin localisation described in this study are consistent with those previously reported in embryos (Phan et al., 2010). Limk1 is present in all neurons of the wild-type developing neural tube at E11.5, with higher levels in the lumbar LMC. P-cofilin is primarily localised to commissural neurons in wild-type mice, although with detectable staining in the LMC (this study). Immunohistochemical analysis confirmed the upregulation of Limk1 throughout the E11.5 neural tube in *pma*/*pma* mutants, particularly obvious in the LMC. Limk1 is a serine/threonine kinase that phosphorylates cofilin, inhibiting its actin filament depolymerisation activity; thus, overexpression of *Limk1* would be predicted to inhibit actin turnover (Sarmiere and Bamburg, 2004). Consistent with this, we showed that motor neurons from the *Limk1*-overexpressing PMA mouse have high levels of p-cofilin and extend axons poorly, in comparison with wild type. *In vivo*, the most severe consequence of this would appear to be loss of the peroneal nerve. To determine empirically whether *Limk1* overactivation can result in neuronal defect, Limk1 activity was mimicked *in ovo* pharmacologically using jasplakinolide to inhibit actin turnover. Delayed or repressed growth of the dorsal-projecting axons was observed in jasplakinolide-treated limbs, indicating that Limk1 pathway dysregulation may disrupt peroneal nerve development. These findings were further confirmed by additional electroporation of LMC *in ovo* to induce *Limk1* overexpression during *in vivo* development of the chicken embryo.

Actin turnover, mediated by Limk1, the ADF/cofilin family, and slingshot proteins, is essential to growth cone motility (Endo et al., 2003; Wen et al., 2007). The importance of Limk1 for CNS neuronal morphology and function has been established (Meng et al., 2002), but the effects of changing Limk1 dosage are context dependent. Short-term overexpression of *Limk1* in cultured hippocampal neurons promotes axon development through cofilin phosphorylation, but longer-term overexpression of *Limk1* leads to growth cone collapse (Rosso et al., 2004). Similarly, in chicken dorsal root ganglia overexpressing *Limk1*, axon extension and growth cone mobility are inhibited (Endo et al., 2003). Phan et al. (2010) showed that overexpression of *LIMK1* in chicken commissural neurons increases p-cofilin levels and stalls commissural growth cones, whereas lowering *LIMK1* accelerates axon extension. The inhibition of commissural growth cone extension could be rescued by co-electroporation of a construct expressing a non-phosphorylatable cofilinS3A mutant. Hence, excessive stabilisation of F-actin at the growth cone either inhibits growth cone dynamics or facilitates myosin-driven growth cone retraction (Gallo et al., 2002).

The fact that *Limk1* is widely expressed in CNS neurons makes it counterintuitive that the PMA mouse has only a hindlimb phenotype. Similarly, *Gdnf*/*Ret* and *Hoxc10*/*d10* double mutants all lead specifically to peroneal nerve loss, despite the expression of these genes in many other neurons (Tarchini et al., 2005; Kramer et al., 2006). Why the peroneal nerve should be overtly susceptible to failure is not known, but we show in this study that this nerve has higher basal levels of phosphorylated (active) Limk1 than the tibial nerve, which suggests that the *pma* mutation raises this further to a level where nerve growth stalls. Limk1 activity should be assayed in the other models above to determine whether this is a general mechanism.

The timing of *Limk1* overexpression overlaps the end of the previously described ‘waiting period’ of the sciatic nerve plexus (Wang and Scott, 2008). This waiting period is characterised by the arrest of axonal growth at the hindlimb sciatic nerve plexus, before limb innervations initiate, mediated through retinoic acid signalling. In *Ret*$^{-/-}$ mice (Kramer et al., 2006), the ventral pathway choice becomes available to dorsal axons that are unable to project dorsally, indicating that delayed axons may also be able to select the ventral

Development (2018) 145, dev160093. doi:10.1242/dev.160093

pathway. Therefore, timing of limb innervation is crucial to correct patterning, and we hypothesise that reduced growth rate of *pma* motor neurons causes dorsal-fated axons to miss their time window for entry to the limb, resulting in atrophied peroneal muscles and clubfoot.

Limk1/EPHA4 interaction

EphA4$^{-/-}$ animals show a similar phenotype to the PMA mice and specifically lack peroneal nerves (Helmbacher et al., 2000). EPHA4/Ephrin-A receptor signalling is known to modulate Limk1 activity: it leads to phosphorylation of ephexin and Src kinases, which signal through small GTPase RhoA and the Rho-associated protein kinase (ROCK) to modulate the phosphorylation of Limk1 and Limk2 (Maekawa et al., 1999; Sahin et al., 2005; Sumi et al., 2001). In addition to the genetic and biochemical interaction between Limk1 and EPHA4 shown here in clubfoot mice, it has also been shown that overactivation of Src kinases redirects dorsal axons to the ventral mesenchyme in the limb (Kao et al., 2009), suggesting a potential 'clubfoot pathway' controlling innervation of the calf muscles.

The PMA mouse as a model of human clubfoot

Previous clinical candidate gene and genome-wide association studies have implicated several loci in the development of clubfoot (Basit and Khoshhal, 2017). These include the hindlimb-specifying genes *PITX1* and *TBX4* described above, members of the limb patterning *HOXA* and *HOXD* clusters (Ester et al., 2009), mutations in genes encoding pro-apoptosis caspases (Ester et al., 2009; Heck et al., 2005), and genes required for normal metabolism of environmental factors, such as folic acid and tobacco smoke (Sharp et al., 2006; Hecht et al., 2007). Collagen (*COL9A1*) and a number of genes encoding muscle contractile proteins may also be mutated in clubfoot, supporting the model of hindlimb rotational arrest resulting from musculoskeletal dysfunction (Liu et al., 2007; Weymouth et al., 2011). The only other gene required for actin cytoskeletal function to have been associated with clubfoot is that encoding Filamin B (Yang et al., 2016). *LIMK1* has not directly been implicated in clubfoot in humans; however, a high incidence of clubfoot occurs in patients with microduplications in chromosome 7q11.23, syntenic with the *pma* candidate region on mouse chromosome 5. Although Williams–Beuren syndrome (deletion of 7q11.23) does not cause clubfoot, patients with duplications of the region have up to a 25% incidence of clubfoot and all patients with microduplications and clubfoot have duplicated *LIMK1* (Torniero et al., 2007; Van der Aa et al., 2009). This is consistent with the link between clubfoot and increased Limk1 activity shown in this study.

Circumstantial and direct anatomical evidence suggests that most patients with clubfoot do have a peroneal nerve but many cases, often associated with a drop-toe phenotype, have a neurological origin, including peroneal nerve palsy (Song et al., 2008; Edmonds and Frick, 2009; Yoshioka et al., 2010). Peroneal nerve dysfunction is rare in clubfoot in humans (8/837 patients in the study by Yoshioka et al., 2010) and the complete peroneal nerve loss described in *pma/pma* mice cannot be regarded as a common cause of clubfoot. Our work outlined in this study, together with other work (N.V., E. Kilby, C.N., S.B., Z.M. and J.M.C., unpublished), is consistent with a hypothesis that muscle loss is the primary cause of clubfoot. Whether the muscle weakness is a direct failure of the muscle, or secondary to other defects, such as failure of vasculature or of nerve function, is perhaps of little consequence to the clubfoot phenotype presented, although the complex clubfoot cases with an underlying neurological basis are among those that do not respond well to normal treatment (i.e. Ponseti manipulation) (Song et al., 2008; Yoshioka et al., 2010). Therefore, identification of the genetic pathway that underlies neurological clubfoot is central to the screening and optimisation of patient care. Upregulation of LIMK1 in human tissue samples cannot be assayed by normal genomic sequencing, but the EPHA4–ephexin–SRC–small GTPase–LIMK1–cofilin pathway has many components that can be screened by simple exome sequencing. Thus, our data support a general model that predisposing mutations in multiple genes in pathways affecting (directly or indirectly) muscle development in the lower limb are causal to clubfoot. The fact that so many such genes exist may well explain why the genetics of clubfoot is so complex in humans.

MATERIALS AND METHODS

Mice and genetic mapping

Experiments were performed under licence after approval by the Aberdeen University Animal Ethical Review Committee. The *pma/pma* homozygotes were obtained from Professor Cheryll Tickle (University of Bath, UK) on an inbred CF1-derived background, and maintained by homozygous mating. The mice were poor breeders, so for generation of experimental animals and controls, the *pma* mutation was bred onto CD1 and C57BL/6 lines. Wild-type CD1 and C57BL/6 mice were used as controls. The PMA phenotype was qualitatively identical irrespective of genetic background, with full bilateral clubfoot. The data presented here are for CD1 background *pma/pma* mice unless stated otherwise (e.g. in the genetic mapping and experiments investigating interaction with EphA4). Embryos were stage matched according to date of gestation, crown-rump length and forelimb morphology. The *pma* mutation produced an idiopathic clubfoot phenotype on all pure and mixed genetic backgrounds.

Epha4$^{+/-}$ mice were obtained from Patrick Charnay (Ecole Normale Supérieure, Paris, France) and maintained on a C57BL/6 background.

For timed matings, the date of vaginal plug was taken as E0.5.

A preliminary pan-genomic screen for informative microsatellite alleles showed that the original *pma* inbred CF1-derived strain maintained by our group was genetically more distinct from BALB/c than from C57BL/6 (Table S4). Therefore, Balb/c crossing was chosen for genetic mapping. Homozygous *pma/pma* male mice on the original inbred CF1-derived background were mated with wild-type BALB/c females, and the F1 *pma/+* progeny crossed to the *pma/pma* males to derive a mixed *pma/pma* and *pma/+* B1 (F2) generation, within which it was inferred would be some informative crossovers to map the *pma* mutation. All mice were scored at birth as 'clubfoot' (inferred *pma/pma*) or 'normal' (inferred *pma/+*). Mice were killed and dissected to confirm the absence or hypotrophy of the peroneal nerve in clubfoot mice and presence of normal peroneal nerve in mice without clubfoot. Tail-tip DNA was isolated from all clubfoot F2 mice (also three non-clubfoot mice, two F1s and both parental strains) by proteinase K digestion (80 µg/ml at 56°C overnight) followed by ethanol precipitation (3:1 ethanol: sample, −20°C for several hours and centrifugation at 12,000 ***g*** for 20 min). Microsatellite genotyping was performed by PCR, using nine primer sets for microsatellites spanning and within the candidate region on chromosome 5 (Table S5). Fluorophore-conjugated forward primers (fluorophores 6FAM, VIC, PET or NED) were synthesised by Eurogentec. PCRs were multiplexed in groups of three using three different fluorophores conjugated to the forward primers (D5Mit218, D5Mit166 and D5Mit428 together; D5Mit282, D5Mit219 and D5Mit60; D5Mit33, D5Mit32 and D5Mit97) (Table S5). Each PCR was run for 35 cycles with an annealing temperature of 61°C and the product sizes analysed using an Applied Biosystems3130 Series Genetic Analyzer. Expected band sizes were determined using DNA from founder *pma/pma* homozygotes and BALB/c mice, as well as their F1 progeny. All PCRs were run on the clubfoot backcross generation mice to identify clubfoot mice that were heterozygous at any of the microsatellite loci, indicative of an informative crossover event.

EphA4 genotyping and crosses

Genomic DNA was isolated from tissue samples by proteinase K digestion using the Qiagen DNA Mini Kit according to the manufacturer's instructions, with elution in 100 µl of buffer AE. Genotyping PCR was

Development (2018) 145, dev160093. doi:10.1242/dev.160093

performed on EphA4-mutant mice and littermates using primers SEK1.1 (5′-TTCTGCCACTGCTATTGGTCACGAG-3′), SEK1.2 (5′-AACTGGT-TCTGAGCTCCAGAAGACC-3′) and SEK1.3 (5′-GATGGGCGCATCG-TAACCGTGCATC-3′), with an annealing temperature of 65°C, for 35 cycles. The EphA4 wild-type allele produced a band of ∼200 bp from primer combination SEK1.1/1.2, and the mutant allele a ∼300 bp band from primer combination SEK1.1/1.3 (Helmbacher et al., 2000).

For study of compound heterozygotes, *EphA4*$^{+/-}$ mice were crossed to *pma/pma* homozygotes to produce *pma/+* heterozygotes that were either *EphA4*$^{+/-}$ or *EphA4*$^{+/+}$. All mice were scored at or before weaning superficially as 'normal', unilateral clubfoot, or bilateral clubfoot. For statistical analysis, to avoid misdiagnosis of gross morphology, all mice from these crosses were dissected and the peroneal nerve was scored as 'normal', 'absent', or 'thin' if a remnant of peroneal nerve was visible (Fig. S13). Nerve scoring was performed blind by an observer unaware of the genotype of the mice.

Gene detection and copy number variation assay

Livers were dissected from one C57BL/6 control mouse and one *pma*/*pma* homozygote, and genomic DNA was isolated from 50 mg samples using the MagMAX DNA Multi-Sample Kit (ThermoFisher Scientific) according to the manufacturer's protocol, with elution into 300 µl volume. gDNA was diluted to 5 ng/µl.

Presence or absence of genes was assayed by genomic PCR using primers for 20 genes described in Table S6.

Copy number variation was assayed by real-time PCR using the TaqMan(R) Copy Number Assay (Applied Biosystems) using manufacturer's validated assays for murine Limk1 (Mm00561325_cn and Mm00165295_cn), Clip2/Cyln2 (Mm00149430_cn), Gtf2ird1 (Mm00158525_cn) and Pde6b, a linked gene that lies outside the *pma* candidate region (Mm00164399_cn). All genes were multiplexed and normalised to the manufacturer's internal reference assay (RNAse P).

Histology and immunohistochemistry

Samples were fixed in 4% paraformaldehyde (PFA) in PBS overnight, washed several times in PBS and dehydrated through a series of ethanol and xylene washes for embedding in paraplast wax embedding medium (Sigma). Wax sections (7 µm) were then cut. For staining, the samples were dewaxed by immersing the slides in histoclear solution (National Diagnostics) and then rehydrated through an ethanol series. Antigen retrieval was performed by boiling slides, 4×5 min, in 0.01 M sodium citrate, pH 6. The samples were blocked in PBS, 4% normal serum, 0.3% bovine serum albumin (BSA) for 1 h. Primary antibody was added and diluted in blocking buffer at 4°C overnight. The primary antibodies used were: anti-β-III-tubulin (T2200, Sigma; 1:1000); anti-PAX6 [PAX6c, Developmental Studies Hybridoma Bank, University of Iowa (DSHB); 1:400]; anti-Cyln1/Clip2 (ab80976, Abcam; 1:200); anti-myosin heavy chain (MF20, DSHB; 1:20); anti-myogenin (F5D-c, DSHB; 1:200); anti-BrdU (ab8955, Abcam; 1:200); anti-Limk1 (611749, BD Transduction Laboratories; 1:200); anti-phospho-LIMK1 (ab38508, Abcam; 1:200); anti-cofilin (ab47401, Abcam; 1:200); anti-phospho-cofilin (sc-21867, Santa Cruz; 1:400); anti-EPHA4 (AF641, R&D Systems; 1:200); anti-EPHB4 (sc-5536, Santa Cruz; 1:100); anti-frizzled 9 (AF2440, R&D Systems; 1:100); anti-islet 1 (sc-23590, Santa Cruz; 1:400); anti-islet 2 (sc-66454, Santa Cruz; 1:400); anti-Pax3 (PAX3-s, DSHB; 1:40); anti-Lmx1b (sc-21231, Santa Cruz; 1:100); anti-Lim1 (4F2, DSHB; 1:20); and anti-neurofilament-associated antigen (3910-s, DSHB; 1:40). No-primary-antibody controls were performed for each antibody. After washing with PBS, fluorescent secondary antibodies were used 1:250 in blocking buffer for 3 h at room temperature as follows (all Molecular Probes, Invitrogen): Alexa594-conjugated chicken anti-rabbit (A21442); Alexa594-conjugated donkey anti-rabbit (A21207); Alexa594-conjugated goat anti-mouse IgG2a (A21135); Alexa594-conjugated goat anti-mouse IgG1 (A21125); Alexa568-conjugated donkey anti-mouse (A10037); Alexa488-conjugated rabbit anti-goat (A11078); Alexa488-conjugated goat anti-mouse IgG2b (A21141); Alexa488-conjugated goat anti-mouse IgG1 (A21121); Alexa488-conjugated donkey anti-rabbit (A21206); and Alexa350-conjugated goat anti-rat (A21093). After PBS washes, the samples were mounted in Vectashield with DAPI (H-1200, Vector Laboratories) to counterstain nuclei.

For immunohistochemistry with a 3,3′-diaminobenzidine (DAB) endpoint, the samples were treated as described above but, before the antigen retrieval, the slides were immersed in 3% H_2O_2 (Sigma-Aldrich) in PBS for 15 min and then washed in PBS for 5 min. The secondary antibodies were biotin-conjugated rabbit anti-mouse (E0354; DakoCytomation) and biotin-conjugated goat anti-rabbit (B7389; Sigma). After PBS washes, the samples were treated with avidin/biotin complex (ABC) reagent ('R.T.U. Vectastain Kit'; Vector Laboratories) and then incubated in 830 µg/ml DAB (Sigma-Aldrich), 20 mM Tris pH 7.4, 0.005% w/v H_2O_2. The DAB reaction was stopped by immersing the samples in running water. The samples were counterstained in Haematoxylin.

Measurement of nerve diameters was performed after dissection and fixation of the sciatic nerve in adult mice approximately midway along the femur. Nerves were fixed in 4% PFA, dehydrated and embedded vertically in wax. Transverse sections (7 µm thick) were cut, rehydrated and stained with Toluidine Blue. Sections were imaged at ×200 on a scale-calibrated Nikon Eclipse 400 light microscope. The diameters of tibial, sural and, if present, peroneal branches of the nerve were measured in at least two places on each of three sections, and the mean total area calculated in µm^2.

Whole-mount antibody staining (immunohistochemistry)

Mouse or chicken embryos were fixed in Dent's fixative (1 part DMSO: 4 parts methanol) for 24 h at 4°C with rocking to permeabilise the tissue. Embryos were bleached with Dent's bleach (1 part H_2O_2: 2 parts Dent's fixative) for 24 h at 4°C with rocking. Embryos were rinsed five times with methanol and post-fixed in Dent's fixative for at least 24 h. Embryos were washed three times with 1×PBS for 1 h, with rocking. Primary antibody, anti-β-III-tubulin (TuJ1, Sigma), was applied at a dilution of 1:1000 in blocking solution (75% 1×PBS, 20% DMSO, 5% donkey serum). β-III-tubulin was used because it is highly expressed in differentiating neurons. Embryos were incubated overnight at room temperature. Embryos were rinsed three times with 1×PBS and then washed five times with 1×PBS for 1 h. Secondary antibody, Alexa 594-donkey anti-rabbit (Molecular Probes), was applied at 1:300 in blocking buffer. Embryos were incubated overnight at room temperature and in the dark.

Embryos were rinsed three times with PBS, then washed with PBS, 5×1 h, 1:1 PBS:methanol, 5 min, and methanol, 3× for 20 min. Following the third methanol wash, half of methanol was removed and replaced with BABB (1 part benzyl alcohol: 2 parts benzyl benzoate) for 5 min. This solution was replaced with 100% BABB and kept at 4°C in the dark. All analyses of the whole-mount IHC results were carried out on a Nikon fluorescence dissecting microscope.

In vivo chicken work

Fertilised White Leghorn eggs (Henry Stewart & Co., Louth, Lincolnshire, UK) were stored at 14°C until needed. To allow embryonic development, eggs were incubated in humidified incubator at 38°C for the required amount of time to reach the desired developmental stage.

Jasplakinolide exposure

A 1 mg/ml solution of jasplakinolide (J4580, Sigma) was prepared in DMSO and diluted to 20 µg/ml with PBS. The eggs were windowed and the stage of the embryo was visually confirmed. Microsponges (1 mm×1 mm) soaked in 20 µg/ml jasplakinolide were placed on the dorsal top of the lumbar and hindlimb regions of HH stage 22 embryos (Fig. S14). Sponges soaked in 2% DMSO were used as vehicle controls. The eggs were closed with adhesive tape and incubated at 38°C for 16 h. Embryos were fixed using Dent's fixative and processed for whole-mount β-III-tubulin immunohistochemistry as described above.

Electroporation

pWZL_Neo_Myr_Flag_LIMK1, expressing full-length Flag-tagged human LIMK1, and control pWZL_Neo_Myr_Flag plasmids were obtained from Addgene (plasmids #20512 and #15300, respectively, deposited by Jean Zhao) and prepared to a concentration of 5 mg/ml using Qiagen Endonuclease-free DNA Maxi Kit. *In ovo* electroporation was performed as described previously (Odani et al., 2008; Nakamura and Funahashi, 2001). LIMK1-Flag DNA or Flag DNA mixed with Fast Green (dye tracer)

Development (2018) 145, dev160093. doi:10.1242/dev.160093

was injected into the lumbar region of the neural tube of HH stage 11 (E1.5) chicken embryos in windowed eggs (Hamburger and Hamilton, 1951). Platinum-coated electrodes spaced at 4 mm were placed on both sides of the injection site, parallel to the long axis of the embryo. The anode was placed on the left of the neural tube and the cathode was placed on the right of the neural tube. Five square pulses (25 volts, 50 ms/s) were applied by a CUY21 electroporator (Nepagene) and the eggs resealed. Surviving embryos were analysed 48-72 h later for whole-mount β-III-tubulin immunohistochemistry, or after a further 5 days for cartilage preparation. Nerve growth was blind-scored independently by two workers, for LIMK1 and control-electroporated embryos, with '0' representing abnormal plexus formation and/or complete failure of axon to project towards the limb, '2' representing normal projection into the limb (Fig. 10), and '1' representing complete or partial failure of projection from at least one lumbar segment.

Alcian Blue cartilage staining

Chicken embryos were fixed overnight in 5% trichloroacetic acid (TCA; Sigma) at 4°C. The next day, the samples were incubated in 0.1% Alcian Blue (Sigma) in 70% ethanol for 8 h and de-stained overnight in 1% HCl in 70% ethanol at 4°C. The embryos were washed 3×1 h in 100% ethanol and then cleared and stored in methyl salicylate (Sigma).

TUNEL

Analysis of apoptosis was performed on tissue sections using the *In situ* Cell Death Detection Kit (fluorescein) (11684795910, Roche Diagnostics) according to the manufacturer's instructions, with permeabilisation using Proteinase K according to instructions. Apoptosis of muscle blocks was quantified manually on transverse sections of the mid-calf of *pma*/*pma* homozygotes and wild-type controls. Each of eight limbs was treated as an independent data point. Four sections were counted per limb, and used to count a mean and standard error of % apoptotic cells for each muscle block in wild types and mutants.

BrdU analysis

Timed pregnant mice were given a single intraperitoneal injection of 10 mg/ml BrdU to label all cells in S phase, and killed 1 h later. Embryos were fixed in 4% PFA, wax embedded and sectioned for anti-BrdU immunohistochemistry using antibodies and conditions as described above.

Motor neuron cultures

E11.5 *pma/pma* and wild-type embryos were stage matched on basis of crown-rump length. The lumbar neural tube was microdissected. The neural tube was further dissected by removing the dorsal region, allowing for purification of the ventral spinal cord, where the LMC neurons are located. A matrix made of bovine collagen (BD Biosciences), rat collagen (BD Biosciences) with DMEM (Gibco) and 20 µl sodium bicarbonate was prepared on a 4-well plate. DEMEM/F12 with 5% foetal bovine serum and 1% pen/strep was used as the culture medium. The dissected neural tube tissue was placed on the collagen matrix and incubated for 3 days at 37°C, 5% CO_2. Fresh culture medium containing 25 mM HEPES buffer was added to the explants before initiating the time-lapse experiment. Time-lapse analysis of growing axons was performed by tracking the movement of multiple growth cones in phase-contrast over a 16 h period using a Leica Inverted microscope at 200× magnification with Volocity imaging software. Full culture conditions are provided in the supplementary Materials and Methods.

Next-generation sequencing and analysis

Genomic DNA was isolated from livers of three Balb/c, three *pma/pma* and two crossover mice (identified by microsatellite analysis above) using DNAzol (ThermoFisher Scientific) according to the manufacturer's instructions. Capture and sequencing of the 2.5 Mb Chr 5p23 region was performed on a contract basis by The GenePool (Next Generation Sequencing and Bioinformatics Platform at the University of Edinburgh, UK). In brief, Illumina sequencing libraries were prepared from each parental strain mouse and the two crossovers. The eArray web-based application (Agilent) was used to design custom DNA baits to capture candidate region sequences. The SureSelect system (Agilent) was used for sequence capture. Captured sequences from each sample were sequenced to at least 30× coverage using 50 bp-end reads on the Illumina platform (GAITx) in-house at The GenePool. Raw sequences were returned to the University of Aberdeen as .gz compressed text files for analysis.

BALB/c sequence reads were aligned to BALB/c reference genome mm9 using bwa (Li and Durbin, 2009), discrepancies identified and a new BALB/c reference generated. The PMA mice and crossovers were then aligned against the new reference and all SNPs and indels identified. Reads were re-aligned around indels and the base quality score recalibrated using GATK (McKenna et al., 2010). Duplicates were marked using Picard (http://broadinstitute.github.io/picard/). SNPs and indels were annotated as exon, intron, untranslated or intergenic sequences. Variant analysis was performed with Samtools 0.1.14 (Li et al., 2009). Annotation of variants was performed with Seqgene v 2.3 (Deng, 2011). SNPs and indels with variant and mapping quality >20 and present in all replicate samples were marked as potentially significant.

Quantitative PCR

For quantitative PCR (qPCR) analysis, neural tubes and hind limbs were microdissected from E11.5 *pma*/*pma* and wild-type C57BL/6 mouse embryos. Total RNA was isolated using the peqGOLD total RNA kit (Peqlab) according to the manufacturer's instructions. cDNA was synthesised by reverse transcription using SuperScript II Reverse Transcriptase kit (Life Technologies) using poly-T primer (Promega). Primers used to amplify genes in the *pma* candidate region were manufactured by Sigma-Aldrich and were as follows: Limk1 forward, 5′-GCTACTTTGTTGCACCTGGAG-3′; Limk1 reverse, 5′-CACACAGGC-AACTCGCTTC-3′; Eif4h forward, 5′-TCAGGAAAGGTGGACCTGAT-3′; Eif4h reverse, 5′-TCCCATCCACCTCTAGATTCTC-3′; Cyln2 forward, 5′-CGGTTCTGCCAACGGTATT-3′; Cyln2 reverse, 5′-GCGGTCAGTG-TTTGTCCTC-3′. qPCR was performed using the Roche Universal Probe system. For each sample, 1 µl of a probe, 0.2 µg cDNA, 10 µl Sensimix (Bioline) and 4 µl DEPC-treated water were combined in each well of a 384-well plate. All reactions were run on a Roche Lightcycler 480 (Roche) and denatured at 95°C for 15 min, followed by 50 cycles of 15 s at 95°C and 30 s at 60°C. All samples were in triplicate and normalised to *Gapdh* in the same run. Statistical analysis of changes in gene expression was performed using the REST statistical package.

Western blot

For western blotting, proteins were extracted from embryonic neural tube and hindlimbs in 5% SDS, 1:100 protease and phosphatase inhibitor cocktails (P2714 and P5726, Sigma-Aldrich) and stored at −20°C. SDS-PAGE was performed in 12% polyacrylamide gels with 10% SDS and proteins were blotted onto nitrocellulose. Membranes were blocked in Tris-buffered saline (TBS) with 0.3% Tween-20 and 10% skimmed milk, and incubated in primary antibody as above, diluted in 2% BSA, 0.05% Tween-20, and TBS overnight at 4°C and washed. Horseradish peroxidase-conjugated species-specific secondary antibody was applied for 1 h before washing in TBS and 0.05% Tween-20, with detection using the enhanced chemiluminescence (ECL) kit (Amersham). Peroxidase-conjugated anti-β-actin (A3854, Sigma) was used as an internal loading control. Secondary antibodies were peroxidase-conjugated anti-rabbit (#7074, Cell Signaling Technology) and peroxidase-conjugated rabbit anti-mouse (A9044, Sigma).

Statistics

The randomisation method of the Relative Expression Software Tool (REST) software was used for qPCR analysis. All error propagation calculations followed the equation:

$$\frac{\Delta z}{z} = \sqrt{\Sigma_1^m \left(\frac{\Delta x_n}{x_n}\right)^2}$$

where z is the mean calculated value, Δz is the calculated standard error of the mean (s.e.m.), x is the experimental value, Δx is the experimental s.e.m., and m is the categories considered.

χ^2 tests were performed online at https://www.graphpad.com. Fisher exact tests were performed online at http://www.socscistatistics.com/tests/fisher/Default2.aspx.

Acknowledgements
We thank Professors Cheryll Tickle and Françoise Helmbacher for discussion and reagents. We thank staff at the Aberdeen Medical Research Facility for specialist technical assistance.

Competing interests
The authors declare no competing or financial interests.

Author contributions
Conceptualization: J.M.C.; Methodology: J.M.C., N.O.L., C.N., K.W., C.M., S.D., Z.M., N.V.; Software: C.M.; Formal analysis: J.M.C., N.O.L., C.N., K.W., C.M., M.N., N.V.; Investigation: J.M.C., N.O.L., C.N., K.W., R.H.C., Z.K.R., A.M.F., I.M., K.O., M.N., S.B., S.D.; Resources: J.M.C.; Data curation: J.M.C.; Writing - original draft: J.M.C., C.N.; Writing - review & editing: N.O.L., C.N., K.W., C.M., R.H.C., Z.K.R., A.M.F., I.M., K.O., M.N., S.B., S.D., Z.M., N.V.; Visualization: J.M.C.; Supervision: J.M.C., Z.M., N.V.; Project administration: J.M.C., S.B., S.D., Z.M., N.V.; Funding acquisition: J.M.C., S.B., Z.M., N.V.

Funding
This study was funded by Medical Research Council project grant reference G0800901 (grant ID: 87379). C.N. was funded by the Fundação para a Ciência e a Tecnologia (Portugal). K.O. was funded by a Gurdon Scholarship from the British Society for Developmental Biology. Z.K.R. was funded by an Anatomical Society Summer Studentship. Deposited in PMC for release after 6 months.

Supplementary information
Supplementary information available online at
http://dev.biologists.org/lookup/doi/10.1242/dev.160093.supplemental

References

Alvarado, D. M., Aferol, H., McCall, K., Huang, J. B., Techy, M., Buchan, J., Cady, J., Gonzales, P. R., Dobb, M. B. and Gurnett, C. A. (2010). Familial clubfoot is associated with recurrent chromosome 17q23.1q23.2 microduplications containing *TBX4*. *Am. J. Hum. Genet.* **87**, 154-160.

Alvarado, D. M., McCall, K., Aferol, H., Silva, M. J., Garbow, J. R., Spees, W. M., Patel, T., Siegel, M., Dobbs, M. B. and Gurnett, C. A. (2011). Pitx1 haploinsufficiency causes clubfoot in humans and a clubfoot-like phenotype in mice. *Hum. Mol. Genet.* **20**, 3943-3952.

Ashby, P. R., Pinconraymond, M., Harris, A., Pinon-Raymond, M. and Harris, A. J. (1993). Regulation of myogenesis in paralyzed muscles in the mouse mutants peroneal muscular atrophy and muscular dysgenesis. *Dev. Biol.* **156**, 529-536.

Bandyopadhyay, U., Cotney, J., Nagy, M., Oh, S., Leng, J., Mahajan, M., Mane, S., Fenton, W. A., Noonan, J. P. and Horwich, J. L. (2013). RNA-Seq profiling of spinal cord motor neurons from a presymptomatic SOD1 ALS mouse. *PLoS ONE* **8**, e53575.

Basit, S. and Khoshhal, K. I. (2017). Genetics of clubfoot; recent progress and future perspectives. *Eur. J. Med. Genet.*, S1769-7212(17)30255-0.

Bayarsaihan, D. and Ruddle, F. H. (2000). Isolation and characterization of BEN, a member of the TFII-I family of DNA-binding proteins containing distinct helix-loop-helix domains. *Proc. Natl. Acad. Sci. USA* **97**, 7342-7347.

Bechtol, C. O. and Mossman, H. W. (1950). Clubfoot: an embryological study of associated muscle abnormalities. *J. Bone Joint Surg. Am.* **32-A**, 827-838.

Bubb, M. R., Spector, I., Breyer, B. B. and Fosen, K. M. (2000). Effects of jasplakinolide on the kinetics of actin polymerization. *J. Biol. Chem.* **275**, 5163-5170.

Capossela, S., Muzio, L., Bertolo, A., Bianchi, V., Dati, G., Chaabane, L., Godi, C., Politi, L. S., Biffo, S., D'Adamo, P. et al. (2012). Growth defects and impaired cognitive-behavioral abilities in mice with knockout for Eif4h, a gene located in the mouse homolog of the Williams-Beuren syndrome critical region. *Am. J. Pathol.* **180**, 1121-1135.

Cartlidge, I. (1984). Observations on the epidemiology of club foot in Polynesian and Caucasian populations. *J. Med. Genet.* **21**, 290-292.

Chantranupong, L., Scaria, S. M., Saxton, R. A., Gygi, M. P., Shen, K., Wyant, G. A., Wang, T., Harper, J. W., Gygi, S. P. and Sabatini, D. M. (2016). The CASTOR proteins are arginine sensors for the mTORC1 pathway. *Cell* **165**, 153-164.

Chapman, C., Stott, N., Port, R. and Nicol, R. (2000). Genetics of club foot in Maori and Pacific people. *J. Med. Genet.* **37**, 680-683.

de Andrade, M., Barnholtz, J. S., Amos, C. I., Lochmiller, C., Scott, A. and Risman, M. (1998). Segregation analysis of idiopathic talipes equinovarus in a Texan population. *Am. J. Hum. Genet.* **79**, 97-102.

Deng, X. (2011). SeqGene: a comprehensive software solution for mining exome- and transcriptome- sequencing data. *BMC Bioinformatics* **12**, 267.

Dickinson, M. E., Flenniken, A. M., Ji, X., Teboul, L., Wong, M. D., White, J. K., Meehan, T. F., Weninger, W. J., Westerberg, H., Adissu, H. et al. (2016). High-throughput discovery of novel developmental phenotypes. *Nature* **537**, 508-514.

Dittrich, R. (1930). Pathogenesis of congenital club-foot (Pes Equinovarus) – an anatomical study. *J. Bone Joint Surg. Am.* **12**, 373-399.

Dobbs, M. B. and Gurnett, C. A. (2013). Genetics of clubfoot. *J. Pediatr. Orthop. B* **21**, 7-9.

Dobbs, M. B., Morcuende, J. A., Gurnett, C. A. and Ponseti, I. V. (2000). Treatment of idiopathic clubfoot: an historical review. *Iowa Orthop. J.* **20**, 59-64.

Duce, S., Madrigale, L., Schmidt, K., Cunningham, C., Liu, G., Barker, S., Tennant, G., Tickle, C., Chudek, S. and Miedzybrodzka, Z. (2010). Micro-magnetic resonance imaging and embryological analysis of wild-type and pma mutant mice with clubfoot. *J. Anat.* **216**, 108-120.

Duce, S. L., D'Alessandro, M., Du, Y., Jagpal, B., Gilbert, F. J., Crichton, L., Barker, S., Collinson, J. M. and Miedzybrodzka, Z. (2013). 3D MRI Analysis of the lower legs of treated idiopathic congenital talipes equinovarus (clubfoot). *PLoS One* **8**, e54100.

Dupressoir, A., Vernochet, C., Bawa, O., Harper, F., Pierron, G., Opolon, P. and Heidmann, T. (2009). Syncytin-A knockout mice demonstrate the critical role in placentation of a fusogenic, endogenous retrovirus-derived, envelope gene. *Proc. Natl. Acad. Sci. USA* **106**, 12127-12132.

Edmonds, E. W. and Frick, S. L. (2009). The drop toe sign: an indicator of neurologic impairment in congenital clubfoot. *Clin. Orthop. Relat. Res.* **467**, 1238-1242.

Endo, M., Ohashi, K., Sasaki, Y., Goshima, Y., Niwa, R., Uemura, T. and Mizuno, K. (2003). Control of growth cone motility and morphology by LIM kinase and Slingshot via phosphorylation and dephosphorylation of cofilin. *J. Neurosci.* **23**, 2527-2537.

Enkhmandakh, B., Makeyev, A. V., Erdenechimev, L., Ruddle, F. H., Chimge, N.-O., Tussie-Luna, M. I., Roy, A. L. and Bayarsaihan, D. (2009). Essential functions of Williams-Beuren syndrome-associated TFII-I genes in embryonic development. *Proc. Natl. Acad. Sci. USA* **106**, 181-186.

Ester, A. R., Weymouth, K. S., Burt, A., Wise, C., Scott, A. Gurnett, C. A., Dobbs, M. B. Blanton, S. H. and Hecht, J. T. (2009). Altered transmission of HOX and apoptotic SNPs identify a potential common pathway for clubfoot. *Am. J. Med. Genet. A* **149A**, 2745-2752.

Flynn, J. M., Ramirez, N., Cornier, A. S. and Colon Negron, E. (2007). Unilateral congenital absence of the calf muscle. *J. Ped. Orthop. Part B* **16**, 70-72.

Francke, U. (1999). Williams-Beuren syndrome: genes and mechanisms. *Hum. Mol. Genet.* **8**, 1947-1954.

Gallo, G., Yee, H. F., Jr and Letourneau, P. C. (2002). Actin turnover is required to prevent axon retraction driven by endogenous actomyosin contractility. *J. Cell Biol.* **158**, 1219-1228.

Gurnett, C. A., Alaee, F., Kruse, L. M., Desruisseau, D. M., Hecht, J. T., Wise, C. A., Bowcock, A. M. and Dobbs, M. B. (2008). Asymmetric lower-limb malformations in individuals with homeobox PITX1 gene mutation. *Am. J. Hum. Genet.* **83**, 616-622.

Hamburger, V. and Hamilton, H. L. (1951). A series of normal stages in the development of the chick embryo. *J. Morphol.* **88**, 49-92.

Hecht, J. T., Ester, A., Scott, A., Wise, C. A., Iovannisci, D. M., Lammer, E. J., Langlois, P. H. and Blanton, S. H. (2007). NAT2 variation and idiopathic talipes equinovarus (clubfoot). *Am. J. Med. Genet. A* **143A**, 2285-2291.

Heck, A. L., Bray, M. S., Scott, A., Blanton, S. H. and Hecht, J. T. (2005). Variation in CASP10 gene is associated with idiopathic talipes equinovarus. *J. Pediatr. Orthop.* **25**, 598-602.

Helmbacher, F., Schneider-Maunoury, S., Topilko, P., Tiret, L. and Charnay, P. (2000). Targeting of the EphA4 tyrosine kinase receptor affects dorsal/ventral pathfinding of limb motor axons. *Development* **127**, 3313-3324.

Hoogenraad, C. C., Eussen, B. H. J., Langeveld, A., van Haperen, R., Winterberg, S., Wouters, C. H., Grosveld, F., De Zeeuw, C. I. and Galjart, N. (1998). The murine CYLN2 gene: genomic organization, chromosome localization, and comparison to the human gene that is located within the 7q11.23 Williams syndrome critical region. *Genomics* **53**, 348-358.

Hoogenraad, C. C., Ahkmanova, A., Grosveld, F., De Zeeuw, C. I. and Galjart, N. (2000). Functional analysis of CLIP-115 and its binding to microtubules. *J. Cell Sci.* **113**, 2285-2297.

Hoogenraad, C. C., Koekkoek, B., Akhmanova, A., Krugers, H., Dortland, B., Miedema, M., van Alphen, A., Kistler, W. M., Jaegle, M., Koutsourakis, M. et al. (2002). Targeted mutation of Cyln2 in the Williams syndrome critical region links CLIP-115 haploinsufficiency to neurodevelopmental abnormalities in mice. *Nat. Genet.* **32**, 116-127.

Huang, G., Massoudi, D., Muir, A. M., Joshi, D. C., Zhang, C.-L., Chiu, S. Y. and Greenspan, D. S. (2017). WBSCR16 is a guanine nucleotide exchange factor important for mitochondrial fusion. *Cell Rep.* **20**, 923-934.

Ippolito, E., De Maio, F., Mancini, F., Bellini, D. and Orefice, A. (2009). Leg muscle atrophy in idiopathic congenital clubfoot: is it primitive or acquired? *J. Child. Orthop.* **3**, 171-178.

Isaacs, H., Handelsman, J. E., Badenhorst, M. and Pickering, A. (1977). The muscles in club foot- a histological, histochemical and electron microscope study. *J. Bone Joint Surg. Br.* **59B**, 465-472.
Iwaki, S., Jensen, B. M. and Gilfillan, A. M. (2007). NTAL/LAB/LAT2. *Int. J. Biochem. Cell Biol.* **39**, 868-873.
Jackson, S. H., Gallin, J. I. and Holland, S. M. (1995). The p47phox mouse knock-out model of chronic granulomatous disease. *J. Exp. Med.* **182**, 751-758.
Jessell, T. M. (2000). Neuronal specification in the spinal cord: Inductive signals and transcriptional codes. *Nat. Rev. Genet.* **1**, 20-29.
Kania, A., Johnson, R. L. and Jessell, T. M. (2000). Coordinate roles of LIM homeobox genes in directing the dorsoventral trajectory of motor axons in the vertebrate limb. *Cell* **102**, 161-173.
Kao, T.-J., Palmesino, E. and Kania, A. (2009). Src family kinases are required for limb trajectory selection by spinal motor axons. *J. Neurosci.* **29**, 5690-5700.
Katoh, H., Watanabe, Y., Ebukuro, M., Muguruma, K., Takabayashi, S. and Shiroishi, T. (2003). Chromosomal mapping of the peroneal muscular atrophy (pma) gene in the mouse. *Exp. Anim.* **52**, 433-436.
Kawano, T., Zhu, M., Troiano, N., Horowitz, M., Bian, J., Gundberg, C., Kolodziejczak, K. and Insogna, K. (2013). LIM kinase 1 deficient mice have reduced bone mass. *Bone* **52**, 70-82.
Kramer, E. R., Knott, L., Su, F., Dessaud, E., Krull, C. E., Helmbacher, F. and Klein, R. (2006). Cooperation between GDNF/Ret and ephrinA/EphA4 signals for motor-axon pathway selection in the limb. *Neuron* **50**, 35-47.
Landmesser, L. (1978). The development of motor projection patterns in the chick hind limb. *J. Physiol.* **284**, 391-414.
Li, H. and Durbin, R. (2009). Fast and accurate short read alignment with Burrows-Wheeler Transform. *Bioinformatics* **25**, 1754-1760.
Li, H., Handsaker, B., Wysoker, A., Fennell, T., Ruan, J., Homer, N., Marth, G., Abecasis, G. and Durbin, R. and 1000 Genome Project Data Processing Subgroup. (2009). The Sequence alignment/map (SAM) format and SAMtools. *Bioinformatics* **25**, 2078-2079.
Lindström, N. O., Neves, C., McIntosh, R., Miedzybrodzka, Z., Vargesson, N. and Collinson, J. M. (2011). Tissue-specific characterization of Lim-kinase 1 expression during mouse embryogenesis. *Gene Expr. Patterns* **11**, 221-232.
Liu, L. Y., Jin, C. L., Cao, D. H., Zhao, N., Lin, C. K. and Sun, K. L. (2007). [Analysis of association between COL9A1 gene and idiopathic congenital talipes equinovarus] (in Chinese). *Yi Chuan.* **29**, 427-432.
Lu, W., Bacino, C. A., Richards, B. S., Alvarez, C., VanderMeer, J. E., Vella, M., Ahituv, N., Sikka, N., Dietz, F. R., Blanton, S. H. et al. (2012). Studies of TBX4 and chromosome 17q23.1q23.2: an uncommon cause of nonsyndromic clubfoot. *Am. J. Med. Genet.* **158A**, 1620-1627.
Maekawa, M., Ishizaki, T., Boku, S., Watanabe, N., Fujita, A., Iwamatsu, A., Obinata, T., Ohashi, K., Mizuno, K. and Narumiya, S. (1999). Signaling from Rho to the actin cytoskeleton through protein kinases ROCK and LIM-kinase. *Science* **285**, 895-898.
McKenna, A., Hanna, M., Banks, E., Sivachenko, A., Cibulskis, K., Kernytsky, A., Garimella, K., Altshuler, D., Gabriel, S., Daly, M. et al. (2010). The genome analysis toolkit: a MapReduce framework for analyzing next-generation DNA sequencing data. *Genome Res.* **20**, 1297-1303.
Meng, Y., Zhang, Y., Tregoubov, V., Janus, C., Cruz, L., Jackson, M., Lu, W. Y., MacDonald, J. F., Wang, J. Y., Falls, D. L. et al. (2002). Abnormal spine morphology and enhanced LTP in LIMK-1 knockout mice. *Neuron* **35**, 121-133.
Miedzybrodzka, Z. (2003). Congenital talipes equinovarus (clubfoot): a disorder of the foot but not the hand. *J. Anat.* **202**, 37-42.
Morris, C. A. (1999). *Williams Syndrome*. In GeneReviews [Internet] (ed. R. A. Pagon, M. P. Adam, H. H. Ardinger, et al.). Seattle, WA: University of Washington, Seattle.
Nakamura, H. and Funahashi, J. (2001). Introduction of DNA into chick embryos by in ovo electroporation. *Methods* **24**, 43-48.
Nonaka, I., Kikuchi, A., Suzuki, T. and Esaki, K. (1986). Hereditary peroneal muscular atrophy in the mouse: an experimental model for congenital contractures (arthrogryposis). *Exp. Neurol.* **91**, 571-579.
Odani, N., Ito, K. and Nakamura, H. (2008). Electroporation as an efficient method of gene transfer. *Dev. Growth Diff.* **50**, 443-448.
Ohno, K., Monji, J., Sasaki, T., Inoue, K. and Shiono, H. (1986). [Congenital absence of the anterior compartment muscle of both legs - a case report] in Japanese. *Nihon Seikeigeka Gakkai Zasshi* **60**, 485-493.
Palmer, S. J., Santucci, N., Widagdo, J., Bontempo, S. J., Taylor, K. M., Tay, E. S. E., Hook, J., Lemckert, F., Gunning, P. W. and Hardeman, E. C. (2010). Negative autoregulation of GTF2IRD1 in Williams-Beuren syndrome via a novel DNA binding mechanism. *J. Biol. Chem.* **285**, 4715-4724.
Palmer, S. J., Taylor, K. M., Santucci, N., Widagdo, J., Chan, Y.-K. A., Yeo, J.-L., Adams, M., Gunning, P. W. and Hardeman, E. C. (2012). *GTF2IRD2* from the Williams–Beuren critical region encodes a mobile-element-derived fusion protein that antagonizes the action of its related family members. *J. Cell Sci.* **125**, 5040-5050.
Peterson, J. F., Ghaloul-Gonzalez, L., Madan-Khetarpal, S., Hartman, J., Surti, U., Rajkovic, A. and Yatsenko, S. A. (2014). Familial microduplication of 17q23.1–q23.2 involving TBX4 is associated with congenital clubfoot and reduced penetrance in females. *Am. J. Med. Genet. A* **164**, 364-369.
Phan, K. D., Hazen, V. M., Frendo, M., Jia, Z. and Butler, S. J. (2010). The bone morphogenetic protein roof plate chemorepellant regulates the rate of commissural axonal growth. *J. Neurosci.* **30**, 15430-15440.
Ponseti, I. V. and Campos, J. (1972). Observations on pathogenesis and treatment of congenital clubfoot. *Clin. Orthop. Relat. Res.* **84**, 50-60.
Porter, M. A., Dobson-Stone, C., Kwok, J. B. J., Schofield, P. R., Beckett, W. and Tassabehji, M. (2012). A role for transcription factor GTF2IRD2 in executive functions in Williams-Beuren Syndrome. *PLoS One* **7**, e47457.
Rebbeck, T. R., Dietz, F. R., Murray, J. C. and Beutow, K. H. (1993). A single-gene explanation for the probability of having idiopathic talipes equinovarus. *Am. J. Hum. Genet.* **53**, 1051-1063.
Rosso, S., Bollati, F., Bisbal, M., Peretti, D. and Sumi, T. (2004). LIMK1 regulates Golgi dynamics, traffic of Golgi-derived vesicles, and process extension in primary cultured neurons. *Mol. Biol. Cell* **15**, 3433-3449.
Sahin, M., Greer, P. L., Lin, M. Z., Poucher, H., Eberhart, J., Schmidt, S., Wright, T. M., Shamah, S. M., O'Connell, S., Cowan, C. W. et al. (2005). Eph-dependent tyrosine phosphorylation of ephexin1 modulates growth cone collapse. *Neuron* **46**, 191-204.
Sarmiere, P. D. and Bamburg, C. R. (2004). Regulation of the neuronal actin cytoskeleton by ADF/cofilin. *J. Neurobiol.* **58**, 103-117.
Sharp, L., Miedzybrodzka, Z., Cardy, A. H., Inglis, J., Madrigal, L., Barker, S., Chesney, D., Clark, C. and Maffulli, N. (2006). The C677T polymorphism in the methylenetetrahydrofolate reductase gene (MTHFR), maternal use of folic acid supplements and risk factor of isolated clubfoot: a case parent triad analysis. *Am. J. Epidemiol.* **164**, 852-861.
Song, K. S., Kang, C. H., Min, B. W., Bae, G. C., Cho, C. H. and Lee, J. H. (2008). Congenital clubfoot with concomitant peroneal nerve palsy in children. *J. Pediatr. Orthop. B* **17**, 85-89.
Stewart, S. F. (1951). Club-foot: its incidence, cause, and treatment; an anatomical-physiological study. *J. Bone Joint Surg. Am.* **33-A**, 577-590.
Sumi, T., Matsumoto, K. and Nakamura, T. (2001). Specific activation of LIM kinase 2 via phosphorylation of threonine 505 by ROCK, a Rho-dependent protein kinase. *J. Biol. Chem.* **276**, 670-676.
Tarchini, B., Huynh, T. H. N., Cox, G. A. and Duboule, D. (2005). HoxD cluster scanning deletions identify multiple defects leading to paralysis in the mouse mutant Ironside. *Genes Dev.* **19**, 2862-2876.
Torniero, C., dalla Bernardina, B., Novara, F., Vetro, A., Ricca, I., Darra, F., Pramparo, T., Guerrini, R. and Zuffardi, O. (2007). Cortical dysplasia of the left temporal lobe might explain severe expressive-language delay in patients with duplication of the Williams-Beuren locus. *Eur. J. Hum. Genet.* **15**, 62-67.
Tursun, B., Schlüter, A., Peters, M. A., Viehweger, B., Ostendorff, H. P., Soosairajah, J., Drung, A., Bossenz, M., Johnsen, S. A., Schweizer, M. et al. (2005). The ubiquitin ligase Rnf6 regulates local Lim kinase 1 levels in axonal growth cones. *Genes Dev.* **19**, 2307-2319.
Van der Aa, N., Rooms, L., Vandeweyer, G., van den Ende, J., Reyniers, E., Fichera, M., Romano, C., Delle Chiaie, B., Mortier, G., Menten, B. et al. (2009). Fourteen new cases contribute to the characterization of the 7q11.23 microduplication syndrome. *Eur. J. Med. Genet.* **52**, 94-100.
VanderMeer, J. E. and Ahituv, N. (2011). cis-regulatory mutations are a genetic cause of human limb malformations. *Dev. Dyn.* **240**, 920-930.
Wagenseil, J. E., Ciliberto, C. H., Knutsen, R. H., Levy, M. A., Kovacs, A. and Mecham, R. P. (2010). The importance of elastin to aortic development in mice. *Am. J. Physiol. Heart Circ. Physiol.* **299**, H257-H264.
Wang, G. and Scott, S. A. (2008). Retinoid signaling is involved in governing the waiting period for axons in chick hindlimb. *Dev. Biol.* **321**, 216-226.
Wang, J. H., Palmer, R. M. and Chung, C. S. (1988). The role of major gene in clubfoot. *Am. J. Hum. Genet.* **42**, 772-776.
Wen, Z., Han, L., Bamburg, J. R., Shim, S., Ming, G. L. and Zheng, J. Q. (2007). BMP gradients steer nerve growth cones by a balancing act of LIM kinase and Slingshot phosphatase on ADF/cofilin. *J. Cell Biol.* **178**, 107-119.
Weymouth, K. S., Blanton, S. H., Bamshad, M. J., Beck, A. E., Alvarez, C., Richards, S., Gurnett, C. A., Dobbs, M. B., Barnes, D., Mitchell, L. E. et al. (2011). Variants in genes that encode muscle contractile proteins influence risk for isolated clubfoot. *Am. J. Med. Genet. A* **155**, 2170-2179.
Yang, N., Higuchi, O., Ohashi, K., Nagata, K., Wada, A., Kangawa, K., Nishida, E. and Mizuno, K. (1998). Cofilin phosphorylation by LIM-kinase 1 and its role in Rac-mediated actin reorganization. *Nature* **393**, 809-812.
Yang, H., Zheng, Z., Cai, H., Li, H., Ye, X., Zhang, X., Wang, Z. and Fu, Q. (2016). Three novel missense mutations in the filamin B gene are associated with isolated congenital talipes equinovarus. *Hum. Genet.* **135**, 1181-1189.
Yoshioka, S., Huisman, N. J. and Morcuende, J. A. (2010). Peroneal nerve dysfunction in patients with complex clubfeet. *Iowa Orthopaedic J.* **30**, 24-28.

SUPPLEMENTARY METHODS

1. Genetic mapping and sequencing of the pma candidate region

The pma mutation was genetically mapped using microsatellites across the previously identified candidate region. Homozygote *pma/pma* founder males were bred with BALB/c females and the [PMA x BALB/c] F1s were backcrossed with *pma/pma* homozygotes. 871 backcross [BALB/c x PMA] F1 x PMA pups were obtained and scored as clubfoot or normal at birth, of which 616 were normal and 255 had clubfoot. This deviated from expected 50:50 ration and is consistent with incomplete penetrance of the phenotype on a mixed genetic background, as described previously (Katoh et al., 1995). Because the genotype of 'normal' pups could not therefore be determined with certainty, 199 clubfoot mice (inferred to be certainly *pma/pma*) were successfully genotyped with a panel of microsatellites (D5Mit 218, D5Mit166, D5Mit 282, D5Mit 219, D5Mit60, D5Mit33, D5Mit32 and D5Mit9 – see Table 1 (main text) and Supplementary Table S1 below) to identify regions of genomic homozygosity associated with the clubfoot phenotype. Two BALB/c founders, two PMA founders (*pma/pma*), 2 [BALB/c x PMA] F1 and 3 'normal' (presumed *pma/+*) [BALB/c x PMA] F1 x PMA backcrosses were also analysed as controls.

There were 12 potentially informative crossovers identified, which located the mutation to 2.5 Mb bounded by D5Mit166 (Chr5:133146598-133146706 bp) and D5Mit60 (Chr5:135715435-135715564 bp) (Figure 6). This reduced candidate region still contained 39 genes. To further define the candidate region, targeted next-generation resequencing was performed on two recombinant mice (one with crossover distal to the mutation, and one proximal to the mutation), three parental *pma/pma* and three parental BALB/c mice. 3.04 Mb encompassing the entire candidate region between D5Mit166 and D5Mit60 was obtained from all mice. Nearly 9000 polymorphic SNPs and indels within this region were interrogated to determine the minimum candidate region within which backcross mice were homozygous for PMA founder alleles. This analysis defined crossovers at approximate positions Chr5: 134514245 and Chr5: 134483438, defining a 0.89 Mb candidate region containing 13 genes: *Gatsl2*; *Wbscr16*; *Gtf2ird2*; *Ncf1*; *Gtf2i*; *Gtf2ird1*; *Cyln2 (Clip2)*; *Lat2*; *Gm52*; *Rfc2*; *Eif4h*; *Limk1* and *Eln*. Within this 0.89 Mb candidate region, nearly 4075 SNPs and small insertions or deletions (indels) were identified that were unambiguously homozygous for the pma allele in all clubfoot crossover animals and not found in BALB/c. Restricting the analysis only to the annotated genes in the region yielded 2053 SNPs and indels, of which 470 were novel mutations that had not previously been identified in any other

mouse line. Any of these could represent the pma mutation and represented too many to analyse indiscriminately. The dataset was therefore filtered to remove any mutation that did not potentially affect the processed mRNA or protein – i.e. intronic sequence and intergenic sequence was removed, and all synonymous coding polymorphisms, though it was recognised that any of these SNPs and indels may still be pathogenic. The refined list contained 23 SNPs that were predicted to cause either nonsynonymous changes in amino acid sequence of the gene product (5 SNPs – Table 2) or changes in the untranslated region of the processed mRNA (18 SNPs, all located in 3' UTR) (Supplementary Table S2). The analysis of these candidates is described in the main text.

2. **Motor neuron explant collagen-cultures.**

Collagen gel was prepared by mixing 180 ml bovine collagen (6 mg/ml) with 180 ml rat collagen solution, 40 ml 10x DMEM culture medium and 20 ml 0.8 M sodium bicarbonate. Gel was kept on ice. 40 ml of collagen gel was dispensed into each well of a 4-well plate. A pipette tip was usd to ensure the gel covered the whole of the well surface. Plates were incubated for 45 minutes at 37°C.

Neural tube was dissected out of sagitally bisected embryos. Neural tube was rotated such that the ventral-most portion faced up, then the neural tube was cut longitudinally to separate the ventrally located motor column from the rest of the spinal cord. The motor column was added to cold culture medium and kept on ice.
Each complete motor column was cut into three equal portions immediately prior to transferring them into the culture dish. 800 µL of culture medium was added to the centre of each wel after the gel had set. The dissected and divided motor column portions were to each well using the 200µL pipette. The portions were in very close proximity to one another. If the portions are too large they settle poorly and if they are too far apart, few axons project. Samples were cultured for 72 hrs at 37°C without moving the plate.

Supplementary Table S1: Full genomic analysis

Click here to Download Table S1

Supplementary Table S2: Filtered mutations

Click here to Download Table S2

Supplementary Table S3: phenotype of pma x EPHA4 compound hets and controls

Click here to Download Table S3

Supplementary Table S4: Pan-genomic microsatellite allele screen

Click here to Download Table S4

Supplementary Table S5: Microsatellite primers and fragment lengths

Primers used for microsatellite fragment length analysis

					Fragment size (bp)	
	Position (Chr5)	**Primer name**	**Labelling**	**Sequence**	**BALB/c**	**PMA**
D5Mit218	132937774-132937901	D5Mit218_F	6FAM	ACATTTATCATTGCTTCTGTTCATG	128	91
		D5Mit218_R		CTGCATTAATACACACAAACATATGC		
D5Mit166	133146598-133146706	D5Mit166_F	VIC	GTGTAAAGTGCAGTTTCTCTGTCTG	109	112
		D5Mit166_R		TCTTCAATTGAGAGTATCTTGTCAGG		
D5Mit428	134150428-134150551	D5Mit428_F	NED	CCTCATGATTTGCTTGGCTT	125	125
		D5Mit428_R		CCATACCTGGGCTGGAGTC		
D5Mit282	135222563-135222664	D5Mit282_F	PET	GTCTTTGCTTGGAGATGTTCG	105	109 (106)
		D5Mit282_R		AACATAGTATGAAACACACACGGG		
D5Mit219	135316925-135317048	D5Mit219_F	6FAM	TGCCTTGTTTCCTATCCACC	122	133 (131)
		D5Mit219_R		GACTATATAGTGAGATCCGGGCC		
D5Mit60	135715435-135715564	D5Mit60_F	VIC	AACCGCATCCATTCCTAGC	132/134	127
		D5Mit60_R		TAAGCACCAAGGAAACCAGG		
D5Mit33	135829291-135829405	D5Mit33_F	NED	ACTCACAACCTTTCTGTCTTAGCC	111	86
		D5Mit33_R		AAACATAATTAGCTGGGCATGG		
D5Mit32	135920110-135920232	D5Mit32_F	PET	TCACTGAGAGATGTGCAGGG	124	137
		D5Mit32_R		AAACTGACCCAGGACTCCG		
D5Mit97	137003596-137003722	D5Mit97_F	6FAM	CAATACAAACGGCAAGACCC	118	124
		D5Mit97_R		CACACAAGTAACTTTAGACGGGG		

Supplementary Table S6: gPCR primer sequences for 20 genes spanning the candidate region.

Primer name	Forward 5'-3'	Reverse 5'-3'
Auts2	GATGACACTGGTAGACTTGC	CTACAGTGCATGAGACCATG
Ras A4	GTTGGCAAACTAGGCCTAAG	GGCAAGTGTACTTGGTAGTC
Dtx2	TGTGAAACACTAGGAGCTGAG	CAGATTCAACTCCTAGCACC
LimK1	CCCTGATGTGACTCATTTGC	GGTTCATTAGGCTTAGCAGC
Serpine1	CAGTAAGAACAACAGGAGCTG	GGCTGACCTTGAATTCATGG
Fzd9	GGCATTGGCTACAACCTGAC	CTCCACGTACTGGAACTTCTC
Ncf1	CACACAGAGATCTATCTGCC	CCTTCTGCAGATACATGGATG
EphB4	GCTCAGAGGATAAAGAGGAC	GTCACAATGCAGATGGTCAG
Hip1	CTAGCATGCACAAAGTTCCG	GTCTCACCCAATACAAAGCG
Gtf2i	CAGTAAGTAAACCAGGAGGC	CAAGAAGAGCTCCAGCTTAC
Trim50	CCGGCTACTGCCCACCCTCT	GACCCCCAAGCGCCAGTCAC
Por	CTTGGCCGACCTGAGCAGCC	AGTCCTGCGCGTTGTCGGTG
Gats	TTGCCAGCGTCGCCAAGGAG	GGCCAGCCAGGTGGCATCAG
Stx1A	CCATGAGGCTCCCGTCCCCA	CGAGTCTTGCCCCGCACTGG
Eln	GGCATGTCTAATCCCGTGCAT	GCGTGCATGCGTGCAATAGCG
Rik	GCTCAAATCGTCGAGGACC	GTGCATGCCGTAAGTCGTGC
Ywhag	CTTGGTGAGTCAGCACTGTC	CGTCATGTCATGTACCATGCAC
cut1	GGCGCCTGACTATACGTG	GGTCAGTCAGTCAGTCTGTAC
fis1	TGCAGCTGCATGCAACGTC	GACTGCCCTGCATGCATGCTAG
Rhbdd2	GTACTGCACGTGCATAAACG	GTACGTGCGGTACGGGTAGGC

FIGURE S1: Vascularisation of muscles in the PMA mouse

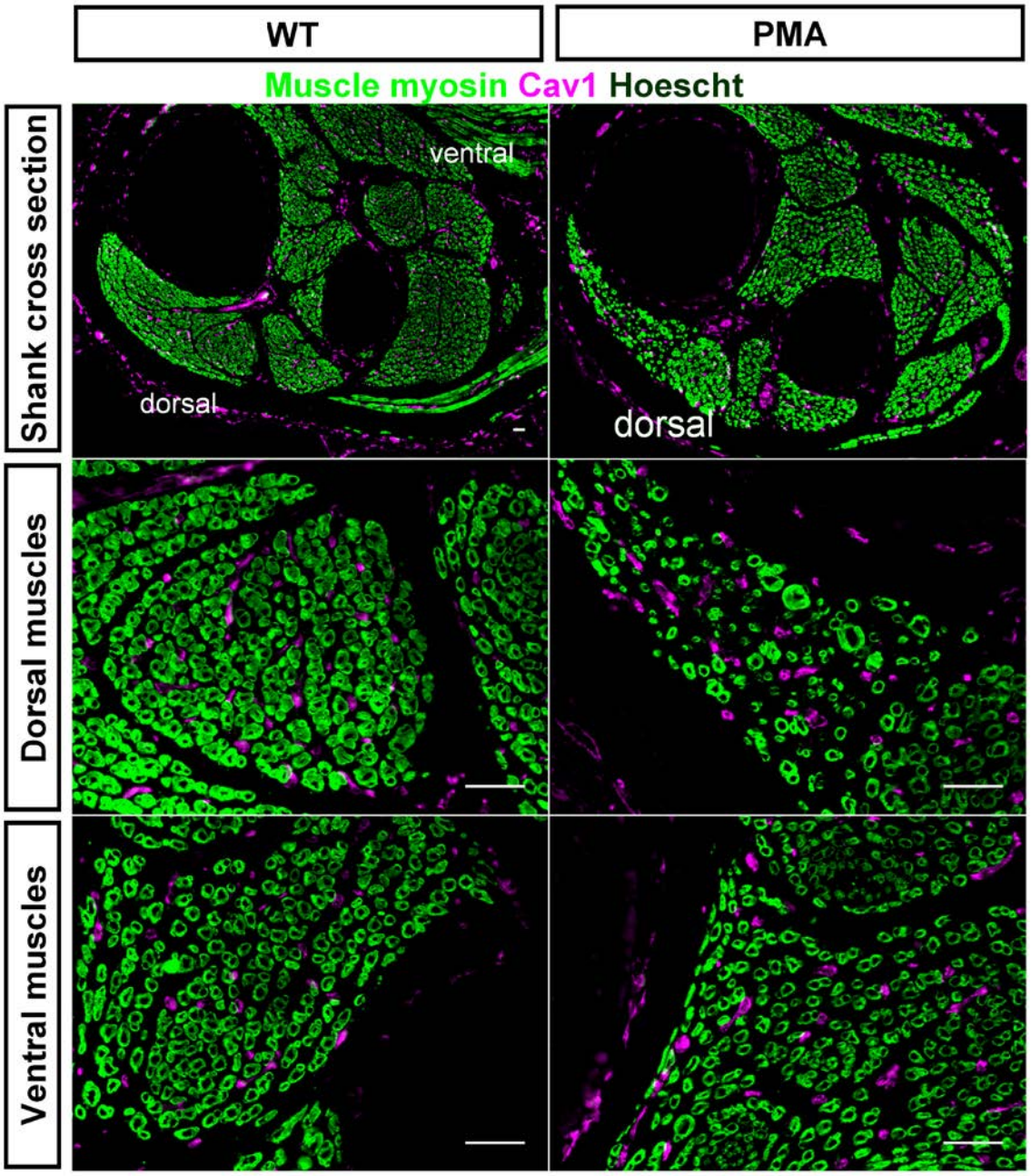

Legend: Immunohistochemistry for blood vessel marker, Caveolin (magenta) and muscle marker, myosin (green) in cross sections of the calf of E16.5 wild-type (left) and *pma/pma* homozygous mice (right). Dorsal and ventral muscles are shown at higher magnification. In contrast to failure of dorsal innervation in *pma/pma* homozygotes (Main text: Figure 1), dorsal muscles are fully vascularised. Scale bar represents 50 μm.

Figure S2: Absence of peroneal nerve in *pma/pma* homozygotes

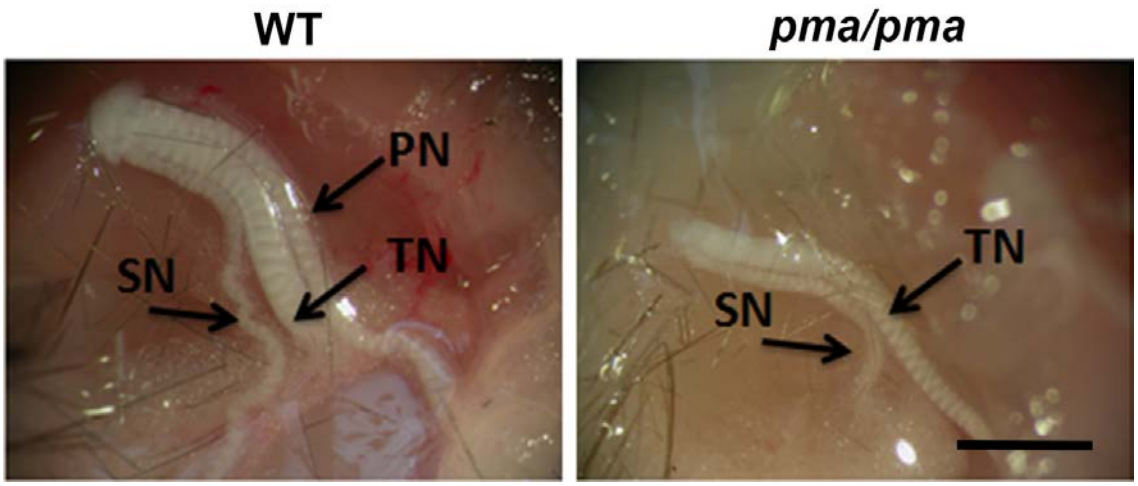

Legend: Dissections of wild-type (left) and pma/pma neonates exposing branches of the sciatic nerve in the hindlimb. The peroneal nerve (PN) is absent in the mutant. Abbreviations: PN, peroneal nerve; TN, tibial nerve; SN, sural nerve. Scale bar represents 4 mm.

Figure S3: Proliferation and cell death in neural tube development in the *pma* embryo

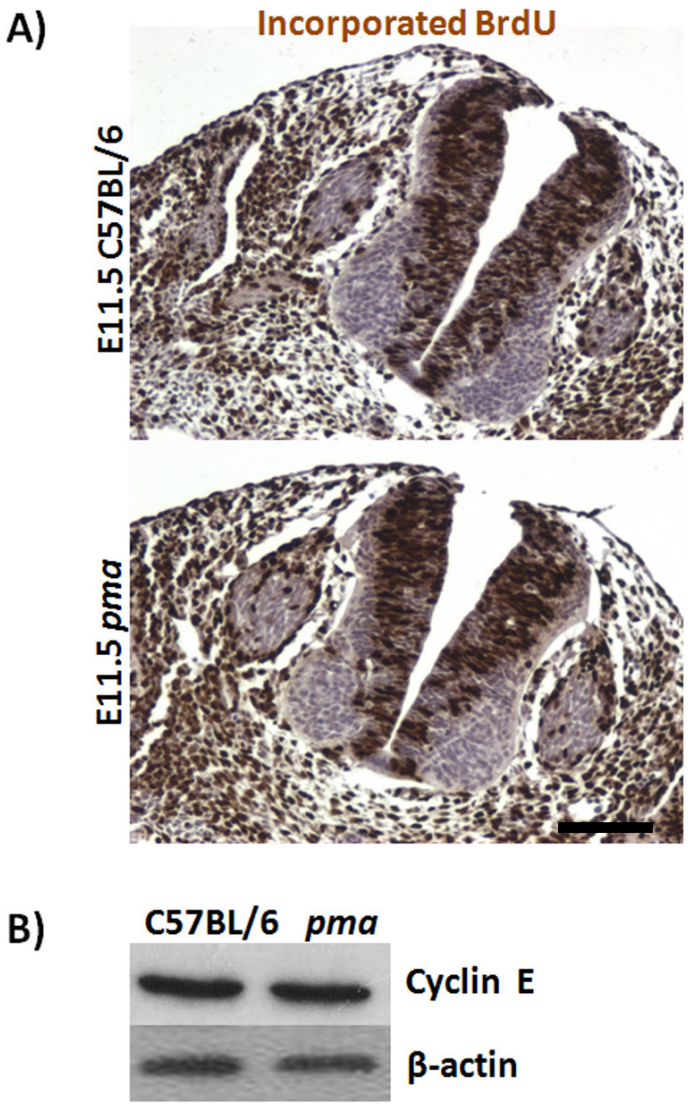

Legend: (A) Incorporation of BrdU (brown) by proliferating neurons in the developing neural tube shows no difference in cell proliferation at E11.5 between the *pma/pma* and wild-type embryos. The sections were counterstained with haematoxylin. The data were not quantified but it was clear there was no gross failure of proliferation in the ventral neural tube of *pma/pma* embryos. (**B)** Mitotic protein Cyclin E was assessed by western blot, but no changes were found between the *pma* and C57BL/6 embryos. β-Actin is shown as a loading control. Scale bar represents 60 μm.

Figure S4 – Expression of developmental genes in pma-mutant hindlimb mesenchyme.

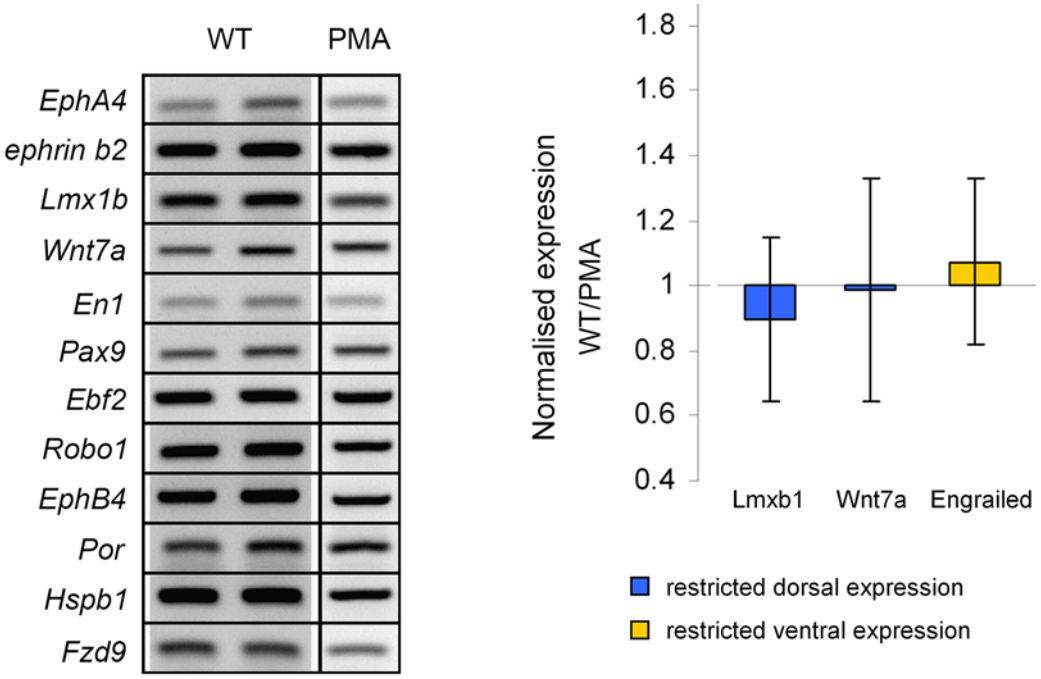

Legend: RTPCR data using cDNA synthesised from E11.5 hindlimbs of wild-type and *pma/pma* embryos. Left – semiquantitative PCR bands for genes that are known to be expressed in the hindlimb in a dorso-ventral restricted pattern (EphA4-Ebf2) and genes on chromosome 5 in the pma region defined by Katoh et al. (1995) (EphB4 – Fzd9). No obvious difference between wild-type and pma mutants. Right – qPCR of normalised gene expression (from three replicates) for dorsal mesenchyme genes, *Lmx1b* and *Wnt7a*, and ventral mesenchyme gene, *En1*. There are no significant differences between genotypes.

Figure S5. Growth cone extension of wild-type and *pma/pma* neurones in culture

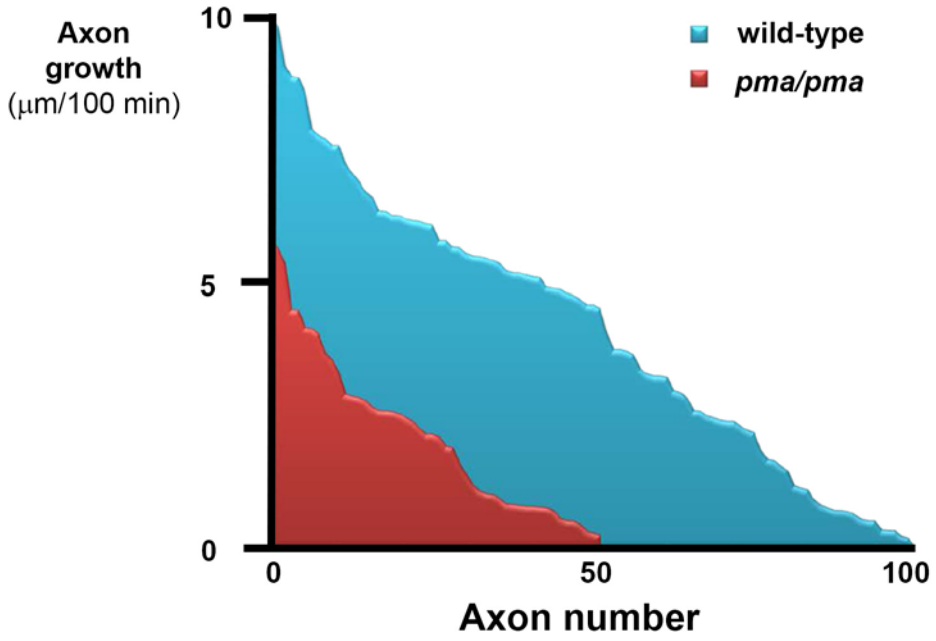

Legend: Growth rate measured in vitro for 97 wild-type and 50 pma/pma lateral motor column (LMC) motor neurones, arranged in order from fastest to slowest. There was very considerable variation in both genotypes, but the distributions were similar, suggesting a general reduction in growth cone extension in pma mutants, independent of their original lateral or medial specification within the LMC.

Figure S6

Genomic PCR for 20 genes across the initial 4.8 Mb candidate region for pma.

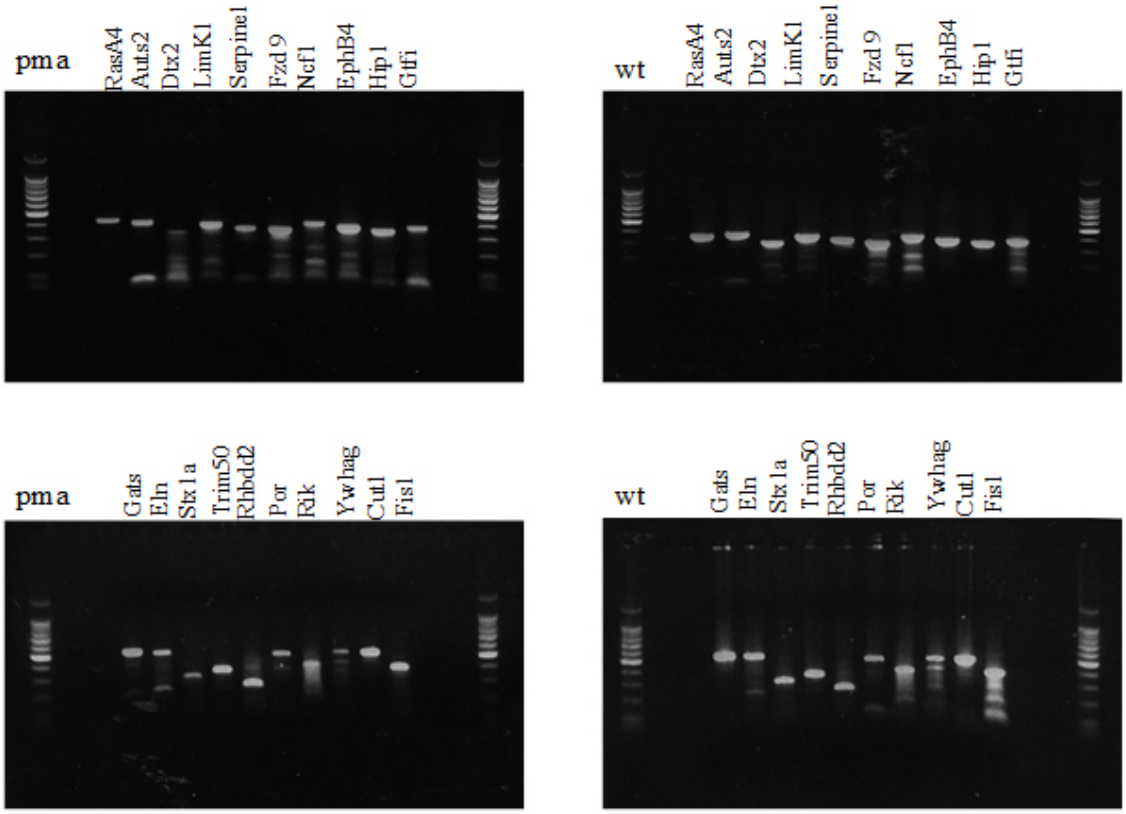

Bands were expected at the following molecular weights: RasA4: 531bp, Auts2: 516bp, Dtx2: 286bp, LimK1: 337bp, Serpine1: 229bp, Fzd9: 474bp, Ncf1: 378bp, EphB4:446bp, Hip1: 508bp, Gtfi: 377bp, Gats: 386bp, Eln: 389bp, Stx1a: 325bp, Trim50: 377bp, Rhbdd2: 347bp, Por: 322bp, Rik: 394bp, Ywhag: 395bp, Cut1: 348bp and Fis1:380bp. The marker is a 100 bp ladder, with the bright band representing 500 bp. All genes were present and all bands were the expected size in pma, suggesting no gross deletions in the region in the mutant mice. PCR primers are listed in Supplementary Table S6.

Figure S7 Micro RNA mmu-miR590-5p

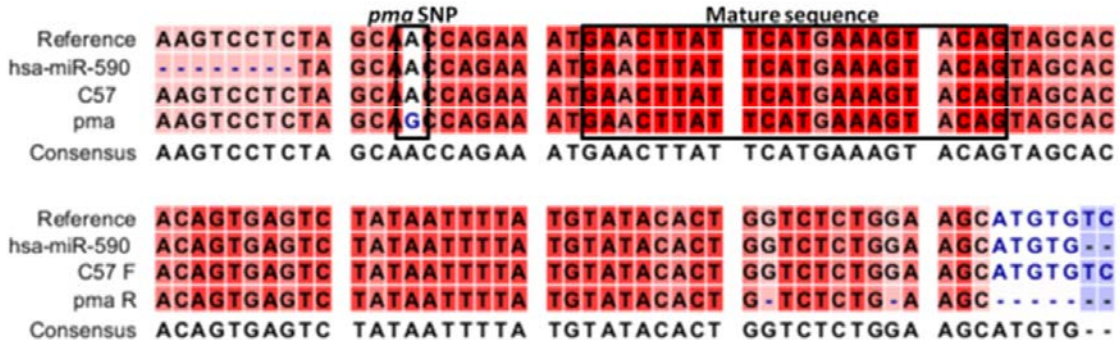

Legend: The sequence of mmu-miR590 in pma mice was investigated by amplifying the core and flanking regions through genomic PCR and compared with both reference BALB/c and C57BL/6 sequence. Sequence of mmu-miR590-5p in pma homozygotes. Reference sequence at top. Has-miR-590 = human sequence. C57 = C57BL/6 sequenced as control. pma = sequence from pma/pma homozygotes. There is a A/A to G/G substitution in PMA animals but this affects a peripheral pre-miRNA nucleotide, predicted not to affect the functional mature sequence which is unchanged.

Figure S8: Copy number analysis of candidate region.

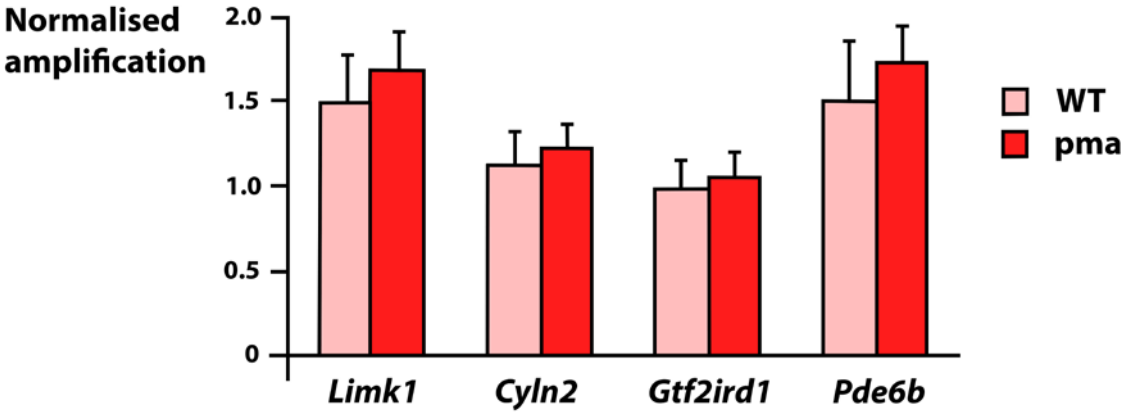

Copy number results based on qPCR of genomic DNA from livers of WT mice and *pma/pma* homozygotes, normalised against reference gene RNAseP. All data are mean ± SEM based on 4 independent replicates. Genes were selected based on position at the proximal (*Gtf2ird1*), central (*Cyln2*) or distal (*Limk1*) part of the candidate region, or linked but 20 Mb outside the candidate region (*Pde6b*). Efficiency of amplification varied between primer sets, but there was no significant difference between wt and *pma/pma* samples at any locus.

Figure S9: Cyln2 (CLIP2) localisation to developing sciatic nerve motor neurons.

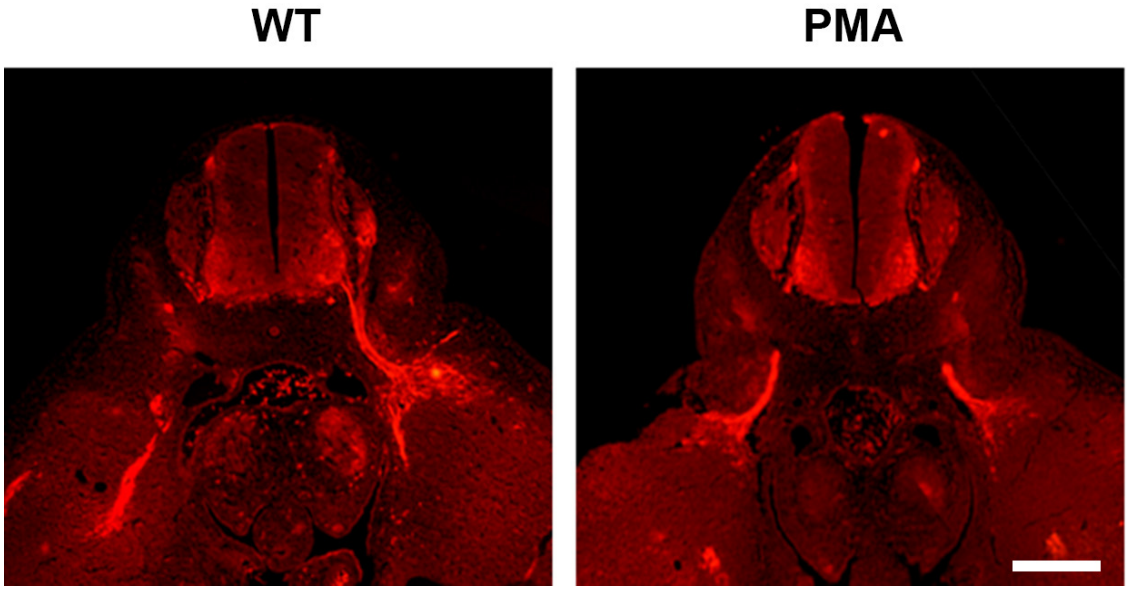

Legend: Fluorescence immunohistochemistry for Cyln2 localisation (red) in E12.5 wild-type (left) and *pma/pma* (right) embryos. Cyln2 is strongly detected in the lateral motor columns and projecting axons of embryos of both genotypes. Scale bar represents 100 μm.

Figure S10: Western blot analysis of PMA embryos at E11.5-E16.5.

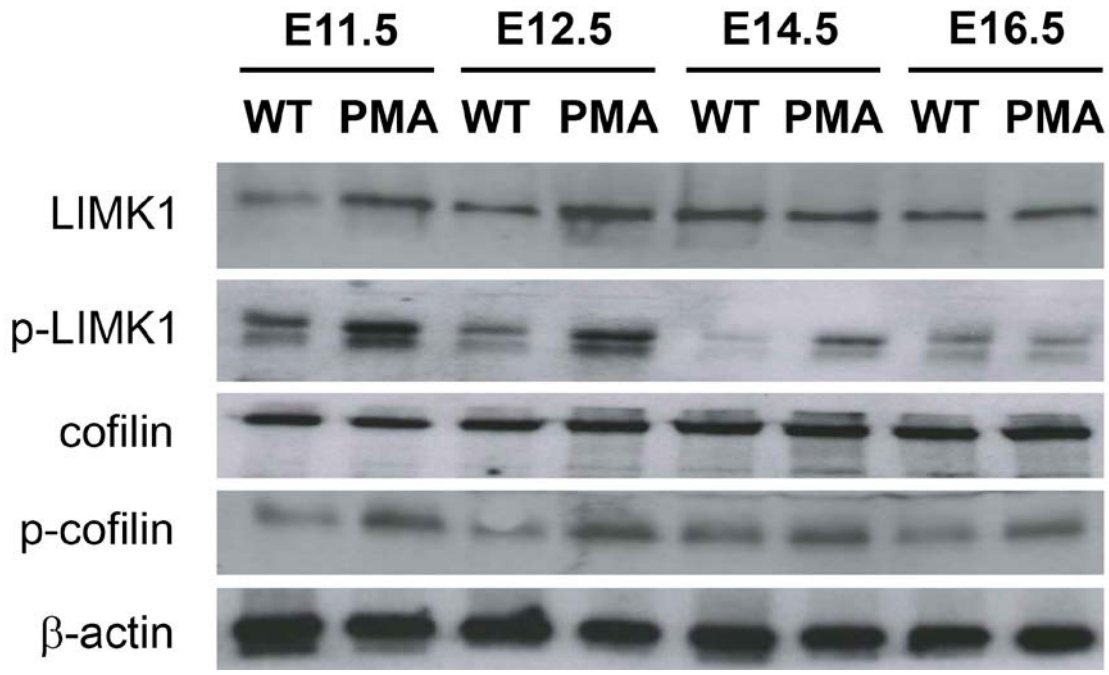

Legend: Western blots (representative of at least 3 replicates) comparing wild-type (WT) with *pma/p*ma (PMA) embryos at E11.5 to E16.5. Total LIMK1 and phosphorylated LIMK1 are quantitatively increased in PMA homozygotes at E11.5 and E12.5, with higher levels of phosphorylated LIMK1 still identifiable at E14.5. Total cofilin levels (a target of LIMK1 kinase activity) are unaffected by genotype, but levels of phosphorylated cofilin increased, consistent with increase in LIMK1 activity. β-actin used as loading control. It is not clear why p-LIMK1 produced a doublet band in this blot, although it may be a result of proteolysis in this particular preparation.

Figure S11: p-LIMK localisation in dorsal and ventral branches of the wild-type sciatic nerve.

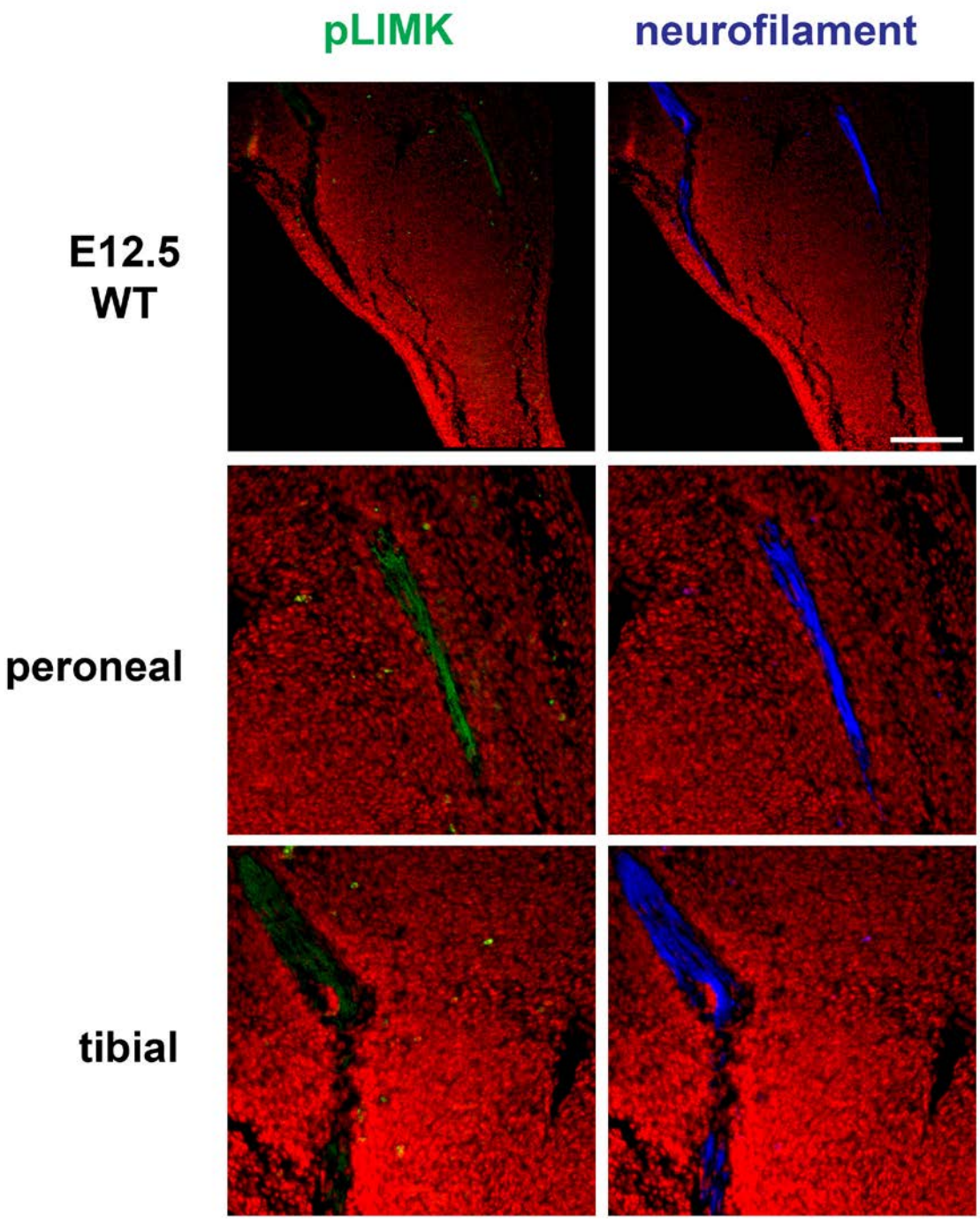

Legend: Immunohistochemical analysis of p-LIMK1 in E12.5 wild-type limb bud. Top row. Double labelling for p-LIMK1 (green), neurofilamant (to label all nerves) (blue). Peroneal branch of the sciatic nerve is at right, tibial branch on right. Bottom two rows are detail of top row, showing peroneal and tibial branches separately. P-LIMK1 levels are higher in peroneal than in tibial nerves. Scale bar represents 400 μm.

Figure S12: Innervation of hindlimbs of EphA4-null mice

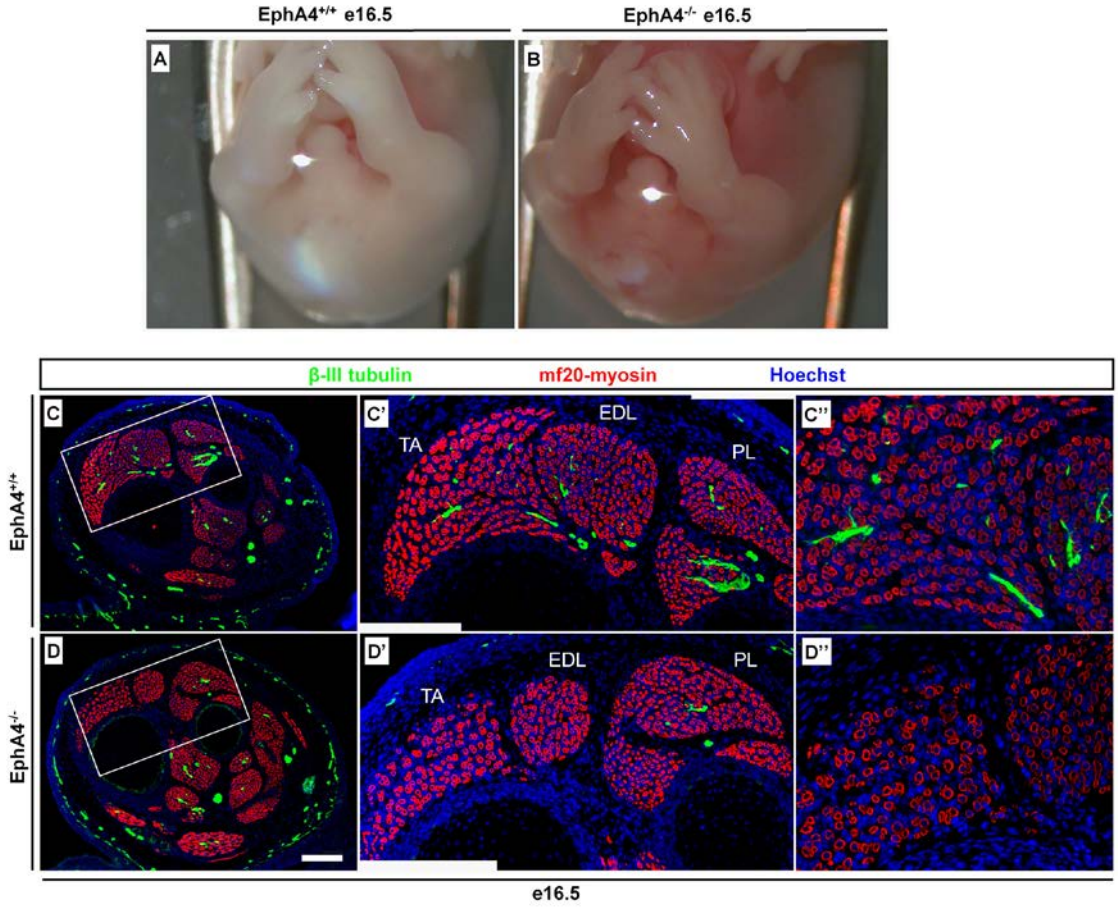

Legend: (A, B) Hindlimbs of E16.5 wild-type (A) and *EphA4*$^{-/-}$ (B) littermates, showing the limb position prior to foot rotation which fails in the mutants. At this developmental stage, the wild-type and mutant foetuses have outwardly indistinguishable limb morphologies. **(C, D)** immunohistochemistry on tissue sections through the lower hindlimbs of wild-type (C-C'') and *EphA4*$^{-/-}$ (D-D'') littermates. Myosin in red, b-III tubulin in green. The tibialis anterior, extensor digitorum longus and peroneum longus are innervated in wild-type, but only the peroneum longus is innervated in the mutant. In contrast, the peroneum longus is not innervated in *pma/pma* (Main text, Figure 1). Abbreviations: TA, tibialis anterior; EDL, extensor digitorum longus; PL, peroneus longus. Scale bar represents 50 μm.

Figure S13: Innervation of hindlimbs of P21 mice from EphA4 x pma crosses

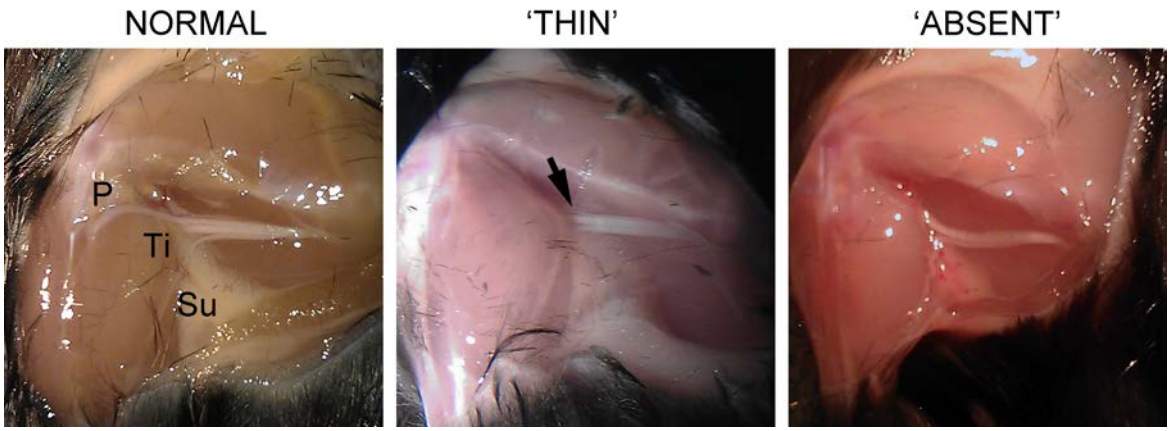

Legend: Representative images of gross dissections of sciatic nerve from: (left panel) legs scored as 'normal' with peroneal (P), Tibial (Ti) and Sural (S) branches visible entering the lower limb muscles; (right panel) leg scored as 'absent' with no evidence of a peroneal nerve, though sural and tibial branches remain visible; (middle panel) in absence of a normal peroneal branch, some limbs scored as 'thin' showed evidence of a very thin dorsal nerve which may be a remnant peroneal branch. See Supplementary Table 4 for full dataset.

FIGURE S14 – Jasplakinolide-soaked microsponge on HH stage 20 chicken embryo